

## LONG TERM STUDY OF THE LIGHT CURVE OF PKS 1510-089 IN GEV ENERGIES

RAJ PRINCE<sup>1</sup>, PRATIK MAJUMDAR<sup>2</sup>, NAYANTARA GUPTA<sup>1</sup>

<sup>1</sup>Raman Research Institute, Sadashivanagar, Bangalore 560080, India

<sup>2</sup>Saha Institute of Nuclear Physics, HBNI, Kolkata, West Bengal 700064, India

*Draft version April 20, 2018*

### ABSTRACT

We have analyzed data from the Flat Spectrum Radio Quasar PKS 1510-089 collected over a period of 8 years from August 2008 to December 2016 with the Fermi-LAT. We have identified several flares of this highly variable source, studied their temporal and spectral properties in detail and compared with previous works on flares of PKS 1510-089. Five major flares and few sub-flares/sub-structures have been identified in our study. The fastest variability time is found to be  $1.30 \pm 0.18$  hr between MJD 55852.063 and 55852.188 where we estimate the minimum size of the emission region to be  $4.85 \times 10^{15}$  cm. In most of the flares the spectral energy distributions are better fitted with Logparabolic distribution compared to simple Power law or Power law with exponential cut-offs. This has strong physics implications regarding the nature of the high energy gamma-ray emission region.

*Keywords:* galaxies: active; gamma rays: galaxies; individuals: PKS 1510-089

### 1. INTRODUCTION

Understanding the physics of blazar flares is one of the most intriguing topics of research in high energy gamma ray astronomy. The origin of flux variability or flares could be in internal shocks in the blazar jets as discussed in earlier studies (Spada et al. 2001). It could also be from perturbation in accretion rate, variations in activity of the central engine (Kelly et al. 2011) or fluctuations in the local magnetic field and particle densities. The observed emissions of different frequencies could be from a single zone or multiple-zones. Depending on the spectral properties of the sources the underlying mechanism of variable emission may vary from one source to another.

PKS 1510-089, located at a redshift of 0.361 (Burbidge & Kinman 1966; Thompson et al. 1990), is highly variable and has been observed in gamma ray energies upto 400 GeV (Abramowski et al. 2013, HESS Collaboration; Aleksić et al. 2014, MAGIC Collaboration). This highly variable Flat Spectrum Radio Quasar (FSRQ) has been monitored by Fermi-LAT over a period of eight years (2008-2016). The multi-wavelength data from flares of PKS 1510-089 during its high state between September 2008 and June 2009 showed variabilities in timescales of 6

to 12 hours (Abdo et al. 2010, Fermi LAT Collaboration). Fermi LAT collaboration recorded isotropic luminosity in gamma rays of approximately  $2 \times 10^{48}$  erg/s on March 26 in 2009. This luminosity exceeds the estimated Eddington's luminosity  $L_{Edd} = 6.86 \times 10^{46}$  erg/s. This is calculated by using the black hole mass given in Abdo et al. 2010. It is hard to find correlation in emissions in different frequencies (Ahnen et al. 2016, MAGIC Collaboration).

The multi-wavelength emission of PKS 1510-089 has been modeled previously in the framework of both leptonic and hadronic models.

In the leptonic model, the low energy component of the spectral energy distribution (SED) is produced by synchrotron radiation of relativistic electrons in the jet. The high energy component is produced by inverse Compton (IC) process where the seed photons can be due to synchrotron radiation (commonly called the Synchrotron Self Compton process) or photons from the Broad Line region (BLR) or dusty torus (DT) (commonly known as the External Compton radiation (EC)). For more details on EC modeling, see Barnacka et al. (2014), Aleksić et al. (2014), Böttcher & Dermer (1998), Tavecchio & Ghisellini (2008).

In hadronic models, the required jet luminosity is high (Böttcher et al. 2013) because pro-

ton cooling is much more inefficient than electron cooling. Proton synchrotron origin of X-ray and gamma-ray emission has been considered recently (Pratim Basumallick & Gupta 2016) to explain the week scale flares (during March-April 2009 and February-April 2012) of PKS 1510-089. In this study they have fitted the radio to gamma ray data with a single zone model of synchrotron emission from electrons and protons for jet luminosity comparable to Böttcher et al. (2013).

The study of light curve and the identification of the location of flares (Tavecchio et al. (2010)) are of much interest due to the wealth of flare data observed by Fermi-LAT. It has been suggested before that there could be multiple simultaneously active gamma ray emission regions along the jet of PKS 1510-089 (Brown 2013). Dotson et al. (2012) discussed about locating the distances of the emission regions of flares from the black hole with the cooling time scales of the energetic electrons. The temperature and density of the seed photons are different in the BLR and molecular torus (MT) regions which determine the inverse Compton cooling regime (Klein - Nishina or Thomson) and time scale of the electrons. The maximum decay time difference of the flares could impose an upper limit on the location of the flares. For luminosity of seed photons in the MT region  $10^{45}$  erg/s and Lorentz factor of the jet  $\Gamma = 10$ , they found the distance of the flare to be within  $2.3 \times 10^{18}$  cm for the Fermi LAT observed flares of energy between 100 MeV to 1 GeV. In a more recent study Dotson et al. (2015) have discussed that the emission regions of 2009 GeV flares of PKS 1510-089 are distributed over a large distance along the length of the jet ranging from the BLR to the MT and to the VLBI radio core zone 10pc away from the black hole.

Due to the extreme nature of variability of the source, the light curve of PKS 1510-089 has shown many interesting results and has been studied by various authors (Abdo et al. 2010; Foschini et al. 2013; Zacharias et al. 2016; Ahnen et al. 2016). However, most of the work that can be found in literature has been focused on the variability studies on short timescales ( $\sim$  few hours to few tens of minutes). As of now, not much effort has been concentrated on study of the long term light curve of the source. In this paper, we aim to address the long term light curve of PKS 1510-089 in the gamma-ray band using the data collected over a period of 8 years with the Fermi-LAT detector.

From the Fermi-LAT data collected over a period of eight years we have selected the high

states/flares of PKS 1510-089 to compare their spectral and temporal properties. Although some of these high states of PKS 1510-089 have been studied before by other authors, a comprehensive study including all the high states observed by Fermi-LAT Collaboration till December, 2016 and a comparison of their spectral and temporal characteristics is not available in literature. Thus our work provides a detailed, complete and updated analysis of the flares of PKS 1510-089 detected by Fermi-LAT. The rest of the paper is organized as follows : in section 2, we describe the data analysis procedures, conduct a detailed study of various flares and construct the spectral energy distributions of the various states of the source. In section 3 we discuss the results and draw conclusions from our analysis.

Throughout the paper we noted the flux in units of  $10^{-6}$  ph/cm<sup>2</sup>/s unless otherwise mentioned.

## 2. FERMI-LAT DATA ANALYSIS OF PKS 1510-089

The Fermi-LAT is a pair conversion  $\gamma$ -ray telescope sensitive to photon energies greater than 20 MeV with a field of view of about 2.4 sr (Atwood et al. 2009). The primary observation mode of Fermi-LAT is survey mode in which the LAT (Large Area Telescope) scans the entire sky every 3 hours. PKS 1510-089 has been continuously monitored by Fermi-LAT since Aug 2008. We consider here the Fermi-LAT data for PKS 1510-089 from 05 Aug 2008–31 Dec 2016 (MJD 54683–57753). The data analysis has been done with the help of *gtlike/pyLikelihood* method, as implemented in the latest version (v10r0p5) of *Fermi Science Tools* software package. In this analysis we have considered photons of energy greater than 100 MeV.

Gamma ( $\gamma$ ) rays are also produced, in the upper atmosphere by the interaction of cosmic rays with ambient medium matter/radiation. In order to reduce the contribution from these  $\gamma$  rays (also called Earth limb  $\gamma$  rays), our analysis is restricted to a maximum zenith angle of  $105^\circ$ . The latest *Fermi Science Tools* include the Instrument Response Function (IRF) “P8R2\_SOURCE\_V6” which has been used in the analysis. The photons are extracted from a circular region of  $10^\circ$  around the source, which is also called the region of interest (ROI). To include all the sources lying within the ROI we have used the third Fermi-LAT catalog (3FGL; Acero et al. 2015). The spectral parameters were left free for sources lying within the  $10^\circ$ . It must be noted that several

other sources are also present in the  $10^\circ$  to  $20^\circ$  ROI. In the model file their spectral parameters have been kept fixed to the 3FGL catalog value. To gauge the significance of  $\gamma$ -ray signal we have done the Maximum Likelihood (ML) test which is defined by  $TS=2\Delta \log(L)$ , where  $L$  is the likelihood function between models with and without a point source at the position of source of interest (Paliya 2015). We have first performed the Maximum Likelihood analysis over the period of interest and for further analysis we have removed the sources of  $TS < 9$  ( $TS = 9$ , corresponds to  $\sim 3 \sigma$  detection; for details see Mattox et al. 1996). The standard background model was used to extract the spectral information. In our analysis, we have also used the latest isotropic background model, “iso\_P8R2\_SOURCE\_V6\_v06”, and the Galactic diffuse emission model, “gll\_iem\_v06”. (available on *Fermi Science Tools* website<sup>1</sup>). The variability of the source can be clearly seen by producing light curves with different time-bins (7 days, 1 day, 12 hr, 6 hr and 3 hr). In Fig.1, we show the weekly light curve which clearly reveals that the source is highly variable. In addition we performed the spectral analysis in the energy range 0.1–300 GeV over several periods of the flaring states by using the *unbinned likelihood analysis*.

The differential photon spectra have been fitted with three different functions whose forms are presented below.

- A power law (PL), defined as

$$dN(E)/dE = N_p(E/E_p)^{-\Gamma}, \quad (1)$$

with  $E_p = 100$  MeV (constant for all the SEDs)

- A log-parabola (LP), defined as

$$dN(E)/dE = N_0(E/E_0)^{-\alpha-\beta \ln(E/E_0)}, \quad (2)$$

with  $E_0 = 300$  MeV (constant for all the SEDs), where  $\alpha$  is the photon index at  $E_0$ ,  $\beta$  is the curvature index and where “ln” is the natural logarithm;

- A power law with an exponential cut-off (PLEC), defined as

$$dN(E)/dE = N_0(E/E_p)^{-\Gamma} \exp(-E/E_c), \quad (3)$$

with  $E_p = 200$  MeV (constant for all the SEDs)

<sup>1</sup> <https://fermi.gsfc.nasa.gov/ssc/data/access/lat/BackgroundModels.html>

## 2.1. Identifying the Flares of PKS 1510-089

PKS 1510-089 is one of the most variable (variability index = 11014.00) blazars in the 3FGL catalog. The variability can be seen in Fig.1, which shows the weekly light curve history of the source observed by the Fermi-LAT during Aug 2008–Dec 2016. Most of the time PKS 1510-089 is in the quiescent state accompanied by occasional periods of high activity where the flux greatly surpasses the quiescent state flux. These episodes of high activity are also referred to as flaring states. The duration of the flaring state is very short (ranging from a few days to a couple of weeks) after which the source returns to its pre-flare quiescent state.

The light curve history of PKS 1510-089 shows that so far there have been five major flaring states (see Fig.1). We refer to these states in our work as Flare-1, Flare-2, Flare-3, Flare-4 and Flare-5 which happened during MJD 54825–55050, MJD 55732–56015, MJD 56505–56626, MJD 57082–57265 and MJD 57657–57753 respectively. We have zoomed out these major flares in bins of 1 day (not shown here) where sub-structures are not clearly seen, 6 hr (primarily for light curve study) and 3 hr (for variability time scale study). The 6 hour binning clearly reveals that there are sub-structures and various phases (pre-flare, plateau, flare and post-flare) inside each individual flare shown in Fig.1. For further study, we concentrate on the plots with 6 hour bins. Two sub-structures have been observed during Flare-1, we label them as flare-1(A) and flare-1(B). Flare-2 shows five sub-structures defined as flare-2(A), 2(B), 2(C), 2(D) and 2(E). No sub-structure was seen during Flare-3 and Flare-5 while three sub-structures were noticed during Flare-4 and defined as flare-4(A), 4(B) and 4(C). All the different phases of activity have been marked with vertical broken red lines (see Fig.2 to Fig.13). The time intervals which have  $TS < 9$  are rejected from the light curve analysis.

## 2.2. Light Curves of Flares

As seen from Fig.1 we can clearly make out five major flaring episodes of PKS 1510-089. We have studied the temporal evolution of each flare separately. In order to show the temporal evolution we have fitted the peaks by a sum of exponentials which give the decay and rising time for the different peaks shown in the light curve plots. The quiescent state (designated by light gray line in the Figs) is also presented in the light curve plots

with the peaks of the flaring states. The functional form of the sum of exponentials is

$$F(t) = 2F_0 \left[ \exp\left(\frac{t_0 - t}{T_r}\right) + \exp\left(\frac{t - t_0}{T_d}\right) \right]^{-1} \quad (4)$$

(Abdo et al. 2010), where  $F_0$  is the flux at time  $t_0$  representing the approximate flare amplitude, and  $T_r$  and  $T_d$  are the rise and decay time of the flare.

### 2.2.1. Flare-1

Fig.2 and Fig.3 show the light curves of flare-1(A) and flare-1(B) in time bins of 6 hr corresponding to the flaring activity during MJD 54890–54927 and MJD 54935–54965 respectively.

In Fig.2 there is no Fermi-LAT data available in the time range MJD 54901.2–54905.6 and before 54899.0 the source was in a quiescent state. We define this quiescent state as the pre-flare epoch of the source. The flaring activity in flare-1(A) can be further divided into two parts—flare(I) and flare(II). The flare(I) phase was observed during MJD 54899.0 to 54910.3 where it shows two peaks P1 and P2 around MJD 54906.4 and 54909.1 with flux  $F_{GeV} = 2.34 \pm 0.40$  and  $2.92 \pm 0.45$  respectively. After this the source resides in a state where the flux exceeds the constant value of  $0.64 \pm 0.07$  for almost 5 days (MJD 54910.3–54915.0). This particular state which is neither the quiescent state nor a fully-fledged flaring state is referred to as the “plateau”. After spending a few days in the so called plateau state (average flux =  $1.38 \pm 0.06$ ) the flux rises again (flare(II)) and shows one major peak P3 at 54916.9 with a flux of  $F_{GeV} = 5.73 \pm 0.50$ . A post-flare phase was also observed during MJD 54921 to 54927 with a flux almost close to that of the quiescent state. The decay and rising time of the peaks are tabulated in Table-1.

A pre-flare was also observed during flare-1(B) (see Fig.3) whose flux of  $F_{GeV} = 0.61 \pm 0.04$  (during time period MJD 54935 to 54944) is in close proximity to that of the quiescent state.

The flaring phase started from MJD  $\sim 54944$  and persisted for  $\sim 7$  days reaching a maximum flux of  $F_{GeV} = 4.49 \pm 0.52$  around MJD 54947.9 (P2). The peak P1 was observed at MJD 54947.4 with a flux of  $F_{GeV} = 3.85 \pm 0.55$ . The peak P2 is followed by two peaks P3 and P4 at MJD 54948.6 and 54949.6 with flux of  $F_{GeV} = 3.25 \pm 0.39$  and  $3.31 \pm 0.40$  respectively. Two post-flares were also observed in the vicinity of the quiescent state. However we did not consider them within the flare

region as the the amplitude of the first one is much lower than the other peaks in the flaring state and the second one is far away from the main flaring phase. However it should be noted that the  $\chi^2$  of the fit improves significantly if these additional small flares are included in the fit. A few outliers were also observed during this epoch for a very short time period (6 hr). The decay and rising time for the peaks are mentioned in Table-1.

### 2.2.2. Flare-2

Similar to Flare-1, we carried out the 6 hr binning of Flare-2 (MJD 55732–56015) which shows the various sub-structures (flare-2(A), flare-2(B), flare-2(C), flare-2(D), flare-2(E)) in various periods which are presented in Fig.4, Fig.5, Fig.6, Fig.7, and Fig.8 respectively.

Five activity phases have been observed in flare-2(A). A pre-flare was observed with a flux close to the quiescent state during the time period MJD 55732.0 to 55737.5. During MJD 55737.5–55741.0 (denoted by flare(I) as was done in the case of Flare-1), the flux starts rising from MJD 55737.9 and goes above 2.0 which is denoted as peak P1 ( $F_{GeV} = 2.26 \pm 0.52$ ) at MJD 55738.9. After spending 3 days in the flare(I) phase the source comes back to its quiescent state. However this duration of quiescence is quite short-lived and the flux starts rising slowly again. This rising part is considered as a plateau which has a time duration of MJD 55741.0 to 55743.5 with a average flux of  $F_{GeV} = 0.79 \pm 0.10$ . The observation period of flare(II) MJD 55743.5 to 55751.0 shows three distinctive peaks P2, P3 and P4 at MJD 55743.9, 55744.9, and 55746.4 with fluxes of  $F_{GeV} = 2.37 \pm 0.55$ ,  $3.67 \pm 1.02$  and  $5.40 \pm 0.60$  respectively. The modeling parameters have been provided in Table-2.

flare-2(B) shows the three phase pattern (pre-flare, flare and post-flare). A pre-flare phase has been observed with flux close to the quiescent state (and it also shows one outlier) and disconnected with the main flare during time period of MJD 55758 to 55765. A flaring activity happened from MJD 55765 to 55771 during which the flux rises upto  $\sim 4.0$ , denoted by peak P1 ( $F_{GeV} = 3.81 \pm 0.46$ ) at MJD 55767.4, and after spending around 5 days in the flaring state it returns to the quiescent state, where the flux is almost similar to that of the pre-flare epoch. The source resides in this quiescent state for a long time and we consider this state as a post-flare from MJD 55771 to 55777. Details of the parameters in these phases are described in Table-2.



The source exhibits a similar three phase pattern during flare-2(C) as well with a variation in the flux in the pre-flare region and the subsequent parameters for modeling this flaring episode is presented in Table-2. Incidentally, one of the brightest flare in the history of PKS 1510-089 (Foschini et al. 2013) was recorded during this period. A major peak P1 ( $F_{GeV} = 17.56 \pm 1.15$ ) was observed at MJD 55853.9 accompanied by a pre-flare and post-flare observed during MJD 55846–55851 and MJD 55855–55860 respectively.

In keeping with the earlier sub-structures flare-2(D) exhibits the typical phase of pre-flare, flare & post-flare. The pre-flare and post-flare were observed during MJD 55860–55866 & MJD 55878–55890. Three major peaks P1, P2, and P3 were observed during the flaring episode where the fluxes were  $F_{GeV} = 6.38 \pm 0.63$ ,  $7.62 \pm 0.73$  and  $8.88 \pm 0.77$  at MJD 55867.9, 55868.4 and 55872.9 respectively. Peak P3 claims the distinction of becoming the 2<sup>nd</sup> highest peak in the history of PKS 1510-089. The modeling parameters have been described in Table-2.

A four phase pattern (pre-flare, flare(I), flare(II) and post-flare) was observed during MJD 55965–56013 which we refer to as flare-2(E). During the pre-flare part slight fluctuations are noticed in the flux around the value 1.0. flare(I) comprises of four distinct major peaks P1, P2, P3 & P4 at MJD 55980.4, 55982.9, 55988.7 and 55990.6 with the fluxes of  $F_{GeV} = 4.20 \pm 0.51$ ,  $4.37 \pm 0.51$ ,  $3.36 \pm 0.44$  &  $4.19 \pm 0.51$  respectively. After spending 4-5 days in an almost quiescent state the flux starts rising again from MJD 55998 and shows a clear and major peak P5 at MJD 56002.4 with a flux of  $F_{GeV} = 2.90 \pm 0.57$ . We refer to this peak as flare(II). During MJD 56005 to 56013 a post-flare was observed whose flux instead of attaining a fixed value keeps fluctuating in the vicinity of the quiescent state flux. The modeling parameters have been described in Table-2.

### 2.2.3. Flare-3

This is the first time that detailed study is being done on the flaring episode of PKS 1510-089 during 10 Sep-13 Oct 2013 referred to as Flare-3. The characteristic temporal evolution of the flux of PKS 1510-089 during Flare-3 can be identified by a four phase pattern (pre-flare, flare(I), flare(II) and post-flare). Fig.9 shows a 6 hr bin light curve encompassing all the four phases and the modeling parameters have been provided in Table-3. The pre-flare phase observed during MJD 56545 to 56552 exhibited a fluctuation in the flux around

$F_{GeV} = 0.54 \pm 0.02$ . flare(I) was observed during MJD 56552–56561, where the flux rises upto 3.5. The three peaks P1, P2 and P3 were observed at MJD 56554.1, 56556.4 and 56557.9 and the corresponding fluxes were  $F_{GeV} = 3.47 \pm 0.47$ ,  $2.72 \pm 0.43$  and  $1.99 \pm 0.49$  respectively. After this flaring state the source spent around 2 days in its quiescent state where the flux was around  $F_{GeV} = 0.54 \pm 0.02$ . The flux again starts rising from MJD 56562.9 and reaches upto  $F_{GeV} = 2.71 \pm 0.45$ , which is shown by peak P4 at MJD 56563.9. After spending around 6 days in 2nd flaring state the source returns to its quiescent state. A post-flare period started from MJD 56570 and continued till MJD 56578 with the flux remaining steadily below 1.0.

### 2.2.4. Flare-4

A 6 hr binning of Flare-4 (MJD 57082–57265) was also carried out by us which revealed the underlying sub-structures with the three distinctive features as flare-4(A), flare-4(B), flare-4(C). Fig.10, Fig.11 and Fig.12 shows these sub-structures along with their different phases.

flare-4(A) displays the usual three phase pattern (pre-flare, flare, post-flare). The details of the phase pattern are described in Table-4. The pre-flare and post-flare were observed before and after the flaring state during MJD 57106–57113 and MJD 57118–57128. Even though there are substantial variations in the flux in both the pre and post flare regions, they are disconnected from the main flare under consideration and are hence not included in the analysis. The flaring duration lasted from MJD 57113 to 57118, during which the flux rose upto a value of 4.5. Two peaks P1 and P2 are clearly seen at MJD 57114.4 and 57115.9 with fluxes of  $F_{GeV} = 3.84 \pm 0.46$  and  $4.47 \pm 0.44$  respectively.

flare-4(B) shows a four phase pattern (pre-flare, flare(I), flare(II), post-flare) with flux variations in the pre-flare region. The detailed study is provided in Table-4. flare(I) was observed during MJD 57155 to 57163 where the flux reached a maximum of  $F_{GeV} = 3.28 \pm 0.41$  (P3). The peaks P1, P2 and P3 at MJD 57156.4, 57158.4 and 57159.9 notch up the peak fluxes of  $F_{GeV} = 2.10 \pm 0.34$ ,  $2.02 \pm 0.33$  and  $3.28 \pm 0.41$  respectively. After spending around 7 days in the flaring state the source descends to its quiescent state where the flux is comparable to the pre-flare value. The source remains in this state for a duration of two and a half days. Surprisingly the flux again starts rising from MJD 57163 and reaches a maximum

flux of  $F_{GeV} = 3.56 \pm 0.47$  (P5). This flare referred to as flare(II) was observed from MJD 57163 to 57171, during which three major peaks P4, P5 and P6 were noticed at MJD 57165.1, 57167.4 and 57170.4. The corresponding fluxes for these peaks were found to be  $F_{GeV} = 2.32 \pm 0.37$ ,  $3.56 \pm 0.47$  and  $3.10 \pm 0.47$  respectively. The post-flare epoch lasted from MJD 57171 to 57177 with a flux of around 1.0.

flare-4(C) was recorded as the 3<sup>rd</sup> brightest flare in the history of PKS 1510-089. The flaring episode lasted from MJD 57242 to 57250 during which the flux rose upto  $\sim 8.60$ . Two major peaks P1 and P2 were observed at MJD 57244.6 and 57245.4 with a flux of  $F_{GeV} = 8.58 \pm 1.03$  and  $6.09 \pm 0.58$  respectively. A pre-flare (MJD 57235 to 57242) and post-flare (MJD 57250 to 57259) were also observed with similar characteristics. For both the pre-flare and post-flare states the flux remains below 1.0. The detail about the parameters have been provided in Table-4.

### 2.2.5. Flare-5

Another flare was observed in Aug-Sep 2016 during MJD 57628–57646. The maximum flux reached  $F_{GeV} = 3.15 \pm 0.47$  with  $TS=236.23$ . Three phase pattern (pre-flare, flare, post-flare) was observed during MJD 57628–57646. A clear peak P1 was observed in the flare phase at MJD 57634.625 (Fig.13). Peak P1 was fitted with the function given in equation (4) and rising and decay time have been provided in Table-5.

All the above peaks during the flaring episodes were fitted with the constant state (value) the details of which are provided in Table-6.

### 2.3. Spectral Energy Distributions of Flares

This section is dedicated to studying the SEDs of flares and also to report the spectral features that will help to recognize different phases of the flares. We have produced the SEDs of PKS 1510-089 during different phases of the flares by using three different models PL, LP and PLEC and their functional forms are given in eqs. 1, 2, and 3 respectively. We note that in all spectral models the choice of reference energy does not affect the spectral shape (Abdo et al. 2010). It is fixed at 100 MeV for PL, at 300 MeV for LP and at 200 MeV for PLEC.

Spectral models (PL, LP and PLEC) have been plotted with the spectral data points in cyan, black and red color respectively. Fig.15 and Fig.16 show the spectral analysis of flare-1(A)

and flare-1(B), their corresponding fitted parameters are given in the Table-7 and Table-8. The  $\log(\text{Likelihood})$  and  $\Delta\log(\text{Likelihood})$  were calculated for each and every phase pattern where  $\Delta\log(\text{Likelihood})$  is defined as  $\Delta\log(\mathcal{L}) = (\log \mathcal{L}(\log\text{-Parabola} / \text{PLEC}) - \log \mathcal{L}(\text{PL}))$ , where  $\mathcal{L} = \text{Likelihood}$ . A progressive spectral hardening have been noticed in flare-1(A) and flare-1(B) with increasing flux from one phase to another.

Hardening in the spectrum is noticed during the flare-2(A), 2(B), 2(C), 2(D) and 2(E) as the flux increases from pre-flare to flare phase. The flare-2(B), 2(C) and 2(D) have shown significant spectral hardening as we move from pre-flare to flare with the value of spectral index  $\Gamma$  changing from  $2.38 \pm 0.08$  to  $2.17 \pm 0.04$ ,  $2.44 \pm 0.06$  to  $2.13 \pm 0.03$  and  $2.65 \pm 0.10$  to  $2.24 \pm 0.02$  when fitted with PL distribution.

The SEDs for all the sub-flares of Flare-2 are plotted in Fig.17 to Fig.21 and the parameters describing all these sub-flares are provided in Table-9 to Table-13.

Flare-3 shows progressive spectral hardening with increasing flux,  $\Gamma=2.47 \pm 0.01$  changes to  $2.35 \pm 0.00$  and  $2.32 \pm 0.01$  (PL fit) which are plotted in Fig.22. The values of the fitted parameters are displayed in Table-14.

A significant amount of spectral hardening is also seen in sub-flares of Flare-4. For flare-4(A) and 4(B) the progressive spectral hardening with increasing flux is seen as  $\Gamma$  decreases from  $2.32 \pm 0.03$  to  $2.14 \pm 0.02$  and  $2.40 \pm 0.05$  to  $2.19 \pm 0.02$  in PL fit. flare-4(C) also shows significant spectral hardening with increasing flux from pre-flare to flare as  $\Gamma$  decreases from  $2.42 \pm 0.09$  to  $1.96 \pm 0.02$  in PL fit. Their SEDs are shown in Fig.23 to Fig.25 and the values of the fitted parameters are provided in Table-15 to Table-17 respectively.

A progressive spectral hardening with increasing flux during pre-flare ( $\Gamma=2.58 \pm 0.08$ ) to flare ( $\Gamma=2.39 \pm 0.04$ ) is also noted in Flare-5. The SED is shown in Fig.26 and the values of the fitted parameters are provided in Table-18.

In Fig.14 we have plotted the photon spectral index as a function of integrated flux ( $F_0$ ) for a few sub-flares. Our plots clearly show spectral hardening with increasing flux. The spectral hardening with increasing flux has been seen previously in many other sources like 3C 454.3 (Britto et al. 2016) and Mrk 501 (Albert et al. 2007).

## 3. RESULTS AND DISCUSSIONS

Being one of the most variable blazars in the Third Source Fermi Catalog (3FGL) the light curve of PKS 1510-089 comprises of five major flares and each flare comprises of several sub-flares. Almost all the sub-flares shows various phases (pre-flare, flare, plateau, post-flare) and the flaring phases consist of peaks of different heights. Decay and rising times have been calculated for the major and clear peaks (P1, P2, P3..etc). Most of the peaks have rising and decay times of few hours (less than a day).

The brightest flare was observed during Oct 2011 at MJD 55853.813. For 3 hr binning the flux was  $F_{GeV} = 25.50 \pm 2.34$  with TS = 1340. A new flare was found in Aug 2015 (Fig.12) which has a peak P1 at MJD 57244.56 with a flux  $F_{GeV} = 8.92 \pm 1.25$  (TS = 397.18). More recently a flare was also observed during 28 Aug–15 Sep, 2016 with a flux of  $F_{GeV} = 3.15 \pm 0.47$  at MJD 57634.61.

Our results show in detail the presence of sub-flares within the flares, which we have scanned separately by using the following function,

$$F(t_2) = F(t_1).2^{(t_2-t_1)/t_d}, \quad (5)$$

to calculate the minimum time of doubling/halving of flux between the time instants  $t_1$  and  $t_2$ ,  $F(t_1)$  and  $F(t_2)$  are respectively the fluxes measured at  $t_1$  and  $t_2$  and  $t_d$  represents the doubling/halving timescale. The results are shown in Table-20 for the 3 hr bin of the light curve. While scanning the light curve the following criteria was used : the flux should be double/half between two consecutive time instants and for these instants of time the condition  $TS > 25$  ( $\sim 5\sigma$  detection) must be satisfied. From Table-20, we find that the shortest observed variability time for the rising part is  $t_{rise} = 1.43 \pm 0.22$  hr between MJD 54945.438 and 54945.563 (flare-1(B)) and for the decaying part  $t_{decay} = 1.30 \pm 0.18$  hr between MJD 55852.063 and 55852.188 (flare-2(C)). There were also some other time intervals within which the flux changed by a factor of 2 but they did not satisfy the requirement of  $TS > 25$ . Such time intervals are ignored in our analysis to find the fastest variability time scale. The hour scale variability time has also been found earlier by Brown (2013) and Saito et al. (2013) for PKS 1510-089. The variability time (The fastest halving/doubling time  $t_d$  is the fastest variability time  $t_{var}$ ) gives an idea about the size of the emission region, if we know the Doppler factor  $\delta$  for the source. Variability time  $t_{var}$ , size of the emission region R and Doppler factor  $\delta$  are

related by

$$R \leq ct_{var}\delta(1+z)^{-1} \quad (6)$$

where  $z$  is the redshift of the source. The redshift corrected variability time ( $\Delta t_{var} = t_{var}(1+z)^{-1}$ ) is used to calculate the size of the emission region while modeling the SEDs of blazars. The apparent speed in the ultrarelativistic jet of PKS 1510-089 has been observed to be upto 46c (Jorstad et al. 2005) which suggests that the Doppler factor could be very high for this source. From equation (6) for  $t_{var} = 1.30$  hr,  $\delta = 47$  (Kadota et al. 2012), we get an emission region of radius  $R \sim 4.85 \times 10^{15}$  cm. A less extreme Doppler factor of 10 would imply an emission region of radius  $R \sim 1.03 \times 10^{15}$  cm. This is comparable to the estimates by Brown (2013) and Saito et al. (2013), which are  $\sim 9.3 \times 10^{15}$  cm and  $\sim 1.5 \times 10^{15}$  cm, respectively. Such small emission regions are rather difficult to accommodate in the standard framework where the emission takes place from a large distance from the central engine (see Tavecchio et al. (2010) and references therein for a more detailed discussion).

A multi-wavelength study of Flare-1 (Mar-Apr 2009) has been done by Abdo et al. (2010). They found that the  $\gamma$ -ray flux had no correlation with the X-ray flux but it showed significant correlation with the optical flux. They also found that the optical flux was lagging 13 days behind the  $\gamma$ -ray flux. Moreover they estimated the isotropic luminosity above 100 MeV during flare (II) of flare-1(A) to be more than  $2 \times 10^{48}$  erg/s. The same flare has also been observed by HESS (Abramowski et al. 2013) in very high energy gamma rays. According to their estimate the integral flux in the very high energy (0.15 - 1.0 TeV) band is  $1.0 \pm 0.2_{stat} \pm 0.2_{sys} \times 10^{-11} cm^{-2} s^{-1}$ , which is  $\approx 3\%$  of the integral flux from Crab nebula. It also shows the steepening in the photon spectrum with spectral index  $5.4 \pm 0.7_{stat} \pm 0.3_{sys}$  for PL distribution. Foschini et al. (2013) have studied the outburst of Oct-Nov 2011. They estimated the shortest variability time ever detected in MeV-GeV energy regime as  $\sim 20$  minutes at MJD 55852, by using the GTI time binning. They have also mentioned about the hour scale variability (see Table-1 of Foschini et al. (2013)) by using the 3 hr time binning which is consistent with the result of Brown (2013) and Saito et al. (2013). We note that our result shows that the shortest variability time is  $\sim 1.30$  hr (by using 3 hr binning) between MJD 55852.063 and 55852.188.

A multi-wavelength study of flare-2(E) has also

been done previously by the MAGIC collaboration (Aleksić et al. 2014). They used the data from Fermi-LAT observations during January 1 to April 7 in 2012 (MJD 55927–56024). Within the time interval MJD 55974 to 55994 they estimated the shortest variability time scale as  $t_{var} = 1.5 \pm 0.6$  hr, which is very close to the value estimated by us  $t_{var} = 1.84 \pm 0.28$  hr (for almost the same time interval) given in Table-20 (flare-2E).

Flare-3 has never been studied in the past. The maximum flux of this flare was found to be around  $F_{GeV} = 3.47 \pm 0.47$  at MJD 56554.1 in our study. The fastest variability time for this flare was estimated as  $t_{var} = 1.98 \pm 0.38$  hr (Table-20, flare-3) which is comparable to the fastest variability time found for other flares.

We have also presented a detailed study of flare-4(A) (MJD 57100–57128) and flare-4(C) (MJD 57235–57259) for the first time where flare-4(C) was identified as the 3<sup>rd</sup> brightest flare in the history of PKS 1510-089. MAGIC collaboration (Ahnen et al. 2016) has previously performed a multi-wavelength study of flare-4(B) observed in May 2015 (MJD 57143–57177).

Flare-5 was found to be a very recent flare of PKS 1510-089. The shortest variability time was calculated as  $t_{var} = 2.00 \pm 0.33$  hr (Table-20).

Figure 27 shows the histogram of the peak fluxes, rise and decay times of the peak fluxes as also enumerated in Table 1-5. The rise and decay times for the different peaks of the flares are distributed around a mean of  $6.04 \pm 0.22$  hr and  $3.88 \pm 0.16$  hr with a standard deviation of 2.40 hr and 2.20 hr respectively, while the peak fluxes are distributed around a mean of  $3.54 \pm 0.08$  with standard deviation of 1.69. Histogram of the constant fluxes are plotted in Fig.28. They are distributed with a mean of  $0.51 \pm 0.01$  and standard deviation of 0.20, which implies that the quiescent state of the source is pretty stable. A frequency distribution of all the flux data points are also plotted in the right hand panel of Figure 28. The plot shows a peaked distribution with slow rising part upto the peak and a fast decaying part beyond the peak. The peak value signifies the flux where the source spends most of the time. Above the peak, the flux values fall rapidly along with a few outliers which can be associated with large flux variations in the source. Tavecchio et al. (2010) have studied flux variations and duty cycles with 1.5 years of data in two of the most variable sources, PKS 1510-089 and 3C 454.3. Our findings with a much larger data set also show very similar behaviour as com-

pared to their study.

In Figure 29, we have plotted the histogram of redshift corrected variability time  $\Delta t_{var}$  (see Table 20). One can clearly see that the distributions for rise and decay are not gaussian but the data points are distributed with mean of  $1.75 \pm 0.02$  hr and  $1.76 \pm 0.02$  hr and with standard deviations of 0.35 hr and 0.40 hr respectively.

Fig.14 shows the variation of photon index as a function of integral fluxes for a few sub-flares. These plots reveal that when the source gets brighter its photon spectrum gets harder, a feature which has been also seen in many other blazars. A similar result was also reported earlier (see Foschini et al. 2013).

We obtained the SEDs for different phases (pre-flare, plateau, flare and post-flare) and fitted them with different functional forms ( differential photon spectrum following PL, LP, PLEC distributions). To get the best fit we calculated the  $\Delta \log(\text{Likelihood})$  and reduced  $\chi^2$  for each phase.

We compared the reduced  $\chi^2$  values for PL, LP and PLEC fits and the spectral cut-off energies in Table-19 for different flares. In almost all the cases, the best fit is found to be LP during flaring episodes. We also note that in the case of PLEC fit, the spectral cut-off energy varies from one flare to another. It is interesting to note that in a few cases where the reduced chi-square values for PLEC are comparable to the values obtained from LP fits, the cut-off energy is well constrained. This has strong physics implications regarding the location of the emission region. If the emission region is close to the core of the source, pair production optical depth would prevent the escape of very high energy gamma rays. As a result the highest energy gamma rays are expected from zones outside the BLR region, in the optically thin outer jet region (see Aleksić et al. 2014, MAGIC Collaboration). The variations in spectral fittings and spectral cut-off energies of the flares indicate that different flares might have originated from different zones along the length of the jet of PKS 1510-089. Earlier studies on blazar flares also indicated the possibility of multiple zones of emission during flares (Brown 2013, Dotson et al. (2012),(2015)). Detailed broadband spectral modeling with photon data ranging from radio to TeV energy would be more useful in exploring the complex nature of flares of this highly variable source.

#### 4. CONCLUDING REMARKS

We have studied the long term light curve of PKS 1510-089 with the data collected by Femi-



LAT between Aug 2008 to Dec 2016. The data have been binned in 7 days, 1 day and 6 hr to explore various features of the light curve. Five major flares along with many substructures have been detected in the weekly binning of the data which have been further studied in detail. From a detailed study on variability, the shortest variability time has been found to be close to 1 hour. This puts a strong constraint on the size of the emission region which has been estimated to be  $\sim 10^{15}$  cm for reasonable values of the Doppler factor. The spectral energy distributions have been fitted with three different functional forms PL, LP and PLEC. We find that in majority of the flares LP gives the best fit and in some cases PLEC can reasonably describe the data. Moreover, when PLEC gives the best fit the cut-off energies are found to vary from one flare to another. Our results indicate that the emission regions vary from one flare to another which is consistent with earlier results.

### 5. ACKNOWLEDGMENT

We thank the referee for insightful comments which improved our work significantly. It is also our pleasure to thank R. J. Britto and V. S. Paliya for many fruitful and helpful discussions on the topic. This work has made use of public Fermi data obtained from the Fermi Science Support Center (FSSC), provided by NASA Goddard Space Flight Center.

### REFERENCES

- Abdo, A. A., Ackermann, M., Agudo, I., et al., 2010, *ApJ*, 721, 1425
- Abdo, A. A., Ackermann, M., Ajello, M., et al., 2010, *ApJ*, 722, 520
- Acero, F., Ackermann, M., Ajello, M., et al., 2015, *ApJS*, 218, 23
- Albert, J., Aliu, E., Anderhub, H., et al., 2007, *ApJ*, 669, 862
- Aleksić, J., Ansoldi, S., Antonelli, L. A., et al., 2014, *A&A*, 569, A46
- Atwood, W. B., Abdo, A. A., Ackermann, M., et al., 2009, *ApJ*, 697, 1071
- Barnacka, A., Moderski, R., Behera, B., Brun, P., & Wagner, S., 2014, *A&A*, 567, A113
- Böttcher, M., & Dermer, C. D., 1998, *ApJL*, 501, L51
- Böttcher, M., Reimer, A., Sweeney, K., & Prakash, A., 2013, *ApJ*, 768, 54
- Britto, R. J., Bottacini, E., Lott, B., Razzaque, S., & Buson, S., 2016, *ApJ*, 830, 162
- Brown, A. M., 2013, *MNRAS*, 431, 824
- Dotson, A., Georganopoulos, M., Kazanas, D., & Perlman, E. S., 2012, *ApJL*, 758, L15
- Dotson, A., Georganopoulos, M., Meyer, E. T., & McCann, K., 2015, *ApJ*, 809, 164
- Burbidge, E. M., & Kinman, T. D., 1966, *ApJ*, 145, 654
- Foschini, L., Bonnoli, G., Ghisellini, G., et al., 2013, *A&A*, 555, A138
- H.E.S.S. Collaboration, Abramowski, A., Acero, F., et al., 2013, *A&A*, 554, A107
- Jorstad, S. G., Marscher, A. P., Lister, M. L., et al., 2005, *AJ*, 130, 1418
- Kadota, A., Fujisawa, K., Sawada-Satoh, S., Wajima, K., & Doi, A. 2012, *PASJ*, 64, 109
- Kelly, B. C., Sobolewska, M., & Siemiginowska, A., 2011, *ApJ*, 730, 52
- MAGIC Collaboration, Ahnen, M. L., Ansoldi, S., et al., 2016, arXiv:1610.09416
- Mattox, J. R., Bertsch, D. L., Chiang, J., et al., 1996, *Apj*, 461, 396
- Paliya, V. S., 2015, *ApJL*, 808, L48
- Pratim Basumallick, P., & Gupta, N., 2017, *Astropart. Phys.*, 88, 1
- Saito, S., Stawarz, L., Tanaka, Y. T., et al., 2013, *ApJL*, 766, L11
- Spada, M., Ghisellini, G., Lazzati, D., & Celotti, A., 2001, *MNRAS*, 325, 1559
- Tavecchio, F., & Ghisellini, G., 2008, *MNRAS*, 386, 945
- Tavecchio, F., Ghisellini, G., Bonnoli, G., & Ghirlanda, G., 2010, *MNRAS*, 405, L94
- Thompson, D. J., Djorgovski, S., & de Carvalho, R., 1990, *PASP*, 102, 1235
- Zacharias, M., Böttcher, M., Chakraborty, N., et al., 2016, arXiv:1611.02098

**Table 1**

Results of temporal fitting with sum of exponentials (equation 4 in the text) for different peaks of the flares (here Flare-1). Column 2 represents the time (in MJD) at which the peaks are observed and the peak fluxes are given in column 3. The fitted rise ( $T_r$ ) and decay ( $T_d$ ) times are mentioned in columns 4 & 5

Peak	$t_0$ [MJD]	flare-1(A)		
		$F_0$ [ $10^{-6}$ ph cm $^{-2}$ s $^{-1}$ ]	$T_r$ [hr]	$T_d$ [hr]
P1	54906.4	2.34±0.40	13.76±7.30	2.06±1.27
P2	54909.1	2.92±0.45	10.97±2.32	7.26±2.25
P3	54916.9	5.73±0.50	10.56±1.58	7.75±0.98
flare-1(B)				
P1	54947.4	3.85±0.55	6.43±2.66	4.04±2.52
P2	54947.9	4.49±0.52	5.71±2.73	2.99±1.23
P3	54948.6	3.25±0.39	1.93±1.98	4.83±2.08
P4	54949.6	3.31±0.40	7.86±2.55	7.85±1.64

**Table 2**

All the columns represent the same parameters as mentioned in Table-1, here results are shown for Flare-2

Peak	$t_0$ [MJD]	flare-2(A)		
		$F_0$ [ $10^{-6}$ ph cm $^{-2}$ s $^{-1}$ ]	$T_r$ [hr]	$T_d$ [hr]
P1	55738.9	2.26±0.52	1.90±1.00	2.67±1.99
P2	55743.9	2.37±0.55	4.70±1.42	3.72±1.44
P3	55744.9	3.67±1.02	4.25±0.93	4.11±0.92
P4	55746.4	5.40±0.60	7.86±0.96	3.98±0.61
flare-2(B)				
P1	55767.4	3.81±0.46	7.38±0.73	5.10±0.72
flare-2(C)				
P1	55853.9	17.56±1.15	2.92±0.89	2.50±0.27
flare-2(D)				
P1	55867.9	6.38±0.63	6.07±1.16	4.74±2.67
P2	55868.4	7.62±0.73	7.08±2.50	3.81±1.43
P3	55872.9	8.88±0.77	5.49±0.75	5.62±0.68
flare-2(E)				
P1	55980.4	4.20±0.51	8.41±1.36	8.78±1.42
P2	55982.9	4.37±0.51	6.91±1.32	2.02±0.65
P3	55988.7	3.36±0.44	7.06±2.86	9.39±1.96
P3	55990.6	4.19±0.51	8.64±1.42	4.46±1.03
P4	56002.4	2.90±0.57	15.07±2.72	9.50±2.29

**Table 3**

All the columns represent the same parameters as mentioned in Table-1, here results are shown for Flare-3

Peak	$t_0$ [MJD]	Flare-3		
		$F_0$ [ $10^{-6}$ ph cm $^{-2}$ s $^{-1}$ ]	$T_r$ [hr]	$T_d$ [hr]
P1	56554.1	3.47±0.47	3.88±0.89	5.16±0.97
P2	56556.4	2.72±0.43	3.94±0.96	7.02±1.28
P3	56557.9	1.99±0.49	3.12±1.21	1.31±0.94
P4	56563.9	2.71±0.45	4.76±0.92	4.88±0.96

**Table 4**

All the columns represent the same parameters as mentioned in Table-1, here results are shown for Flare-4

Peak	$t_0$ [MJD]	flare-4(A)		
		$F_0$ [ $10^{-6}$ ph cm $^{-2}$ s $^{-1}$ ]	$T_r$ [hr]	$T_d$ [hr]
P1	57114.4	3.84±0.46	8.29±1.69	4.93±2.40
P2	57115.9	4.47±0.44	8.27±2.98	18.10±2.27
flare-4(B)				
P1	57156.4	2.10±0.34	6.83±2.12	9.50±3.99
P2	57158.4	2.02±0.33	11.77±4.48	9.49±3.84
P3	57159.9	3.28±0.41	8.00±2.27	5.35±2.92
P4	57165.1	2.32±0.37	9.87±1.83	3.99±1.56
P5	57167.4	3.56±0.47	6.35±2.09	11.82±1.61
P6	57170.4	3.10±0.47	8.53±1.60	2.67±0.87
flare-4(C)				
P1	57244.6	8.58±1.03	7.59±0.85	2.66±0.98
P2	57245.4	6.09±0.58	7.11±1.68	2.86±0.80

**Table 5**

All the columns represent the same parameters as mentioned in Table-1, results are shown here for Flare-5

Peak	$t_0$ [MJD]	Flare-5		
		$F_0$ [ $10^{-6}$ ph cm $^{-2}$ s $^{-1}$ ]	$T_r$ [hr]	$T_d$ [hr]
P1	57634.6	3.15±0.47	8.96±1.06	6.28±0.89

**Table 6**

The values of constant flux which are also fitted with the above peaks in the light curve. A histogram of the constant fluxes in different periods is shown in left panel of Figure 28

Flares/Sub-flares	Constant flux Flux $F_{0.1-300 \text{ GeV}}$ [ $10^{-6} \text{ ph cm}^{-2} \text{ s}^{-1}$ ]
flare-1(A)	0.64±0.07
flare-1(B)	0.61±0.04
flare-2(A)	0.15±0.03
flare-2(B)	0.35±0.03
flare-2(C)	0.74±0.09
flare-2(D)	0.53±0.05
flare-2(E)	0.88±0.04
Flare-3	0.54±0.02
flare-4(A)	0.69±0.05
flare-4(B)	0.50±0.04
flare-4(C)	0.41±0.04
Flare-5	0.74±0.04

**Table 7**

Results of SEDs fitted with different spectral types like PL, LP, PLEC. Different periods of activity of the flares (here flare-1(A)) are mentioned in the 1st column. The fitted fluxes and the spectral indices are shown in the columns 2 & 3. The goodness of unbinned fits by log(Likelihood) is given in column 5 and the  $\Delta\log(\text{Likelihood})$  is calculated with respect to the log(Likelihood) of the PL fit (see text for more details).

Activity	$F_{0.1-300 \text{ GeV}}$ ( $10^{-6} \text{ ph cm}^{-2} \text{ s}^{-1}$ )	PowerLaw (PL) $\Gamma$		-log(Likelihood)	
pre-flare	0.45±0.06	2.41±0.11	-	24496.5	-
flare(I)	3.73±0.15	2.30±0.04	-	20608.5	-
plateau	3.26±0.14	2.29±0.04	-	20170.3	-
flare(II)	4.57±0.12	2.24±0.02	-	38286.7	-
post-flare	2.27±0.10	2.52±0.05	-	24715.6	-
Activity	$F_{0.1-300 \text{ GeV}}$ ( $10^{-6} \text{ ph cm}^{-2} \text{ s}^{-1}$ )	LogParabola (LP) $\alpha$	$\beta$	-log(Likelihood)	$\Delta\log(\text{Likelihood})$
pre-flare	0.44±0.06	2.40±0.15	0.00±0.00	24496.5	0.0
flare(I)	3.72±0.15	2.28±0.05	0.00±0.00	20608.5	0.0
plateau	3.18±0.14	2.18±0.06	0.08±0.03	20166.4	-3.9
flare(II)	4.45±0.12	2.14±0.04	0.07±0.02	38279.2	-7.5
post-flare	2.24±0.10	2.46±0.06	0.06±0.04	24714.2	-1.4
Activity	$F_{0.1-300 \text{ GeV}}$ ( $10^{-6} \text{ ph cm}^{-2} \text{ s}^{-1}$ )	PLExCutoff (PLEC) $\Gamma_{PLEC}$	$E_{cutoff}$ [GeV]	-log(Likelihood)	$\Delta\log(\text{Likelihood})$
pre-flare	0.44±0.06	2.32±0.15	9.359±7.506	24496.3	-0.2
flare(I)	3.71±0.15	2.26±0.04	30.000±0.253	20610.0	1.5
plateau	3.18±0.14	2.11±0.08	5.185 ±2.394	20164.8	-5.5
flare(II)	4.50±0.12	2.16±0.04	15.980±6.358	38281.0	-5.7
post-flare	2.24±0.10	2.40±0.08	6.081±3.856	24713.4	-2.2

**Table 8**

All the columns represent the same parameters as mentioned in Table-7, here results are shown for flare-1(B)

Activity	$F_{0.1-300 \text{ GeV}}$ ( $10^{-6} \text{ ph cm}^{-2} \text{ s}^{-1}$ )	PowerLaw (PL) $\Gamma$		-log(Likelihood)	
pre-flare	1.12 ± 0.07	2.50 ± 0.06	-	33110.1	-
flare	5.20 ± 0.15	2.41 ± 0.03	-	36271.2	-
post-flare	2.56 ± 0.09	2.33 ± 0.03	-	49194.4	-
Activity	$F_{0.1-300 \text{ GeV}}$ ( $10^{-6} \text{ ph cm}^{-2} \text{ s}^{-1}$ )	LogParabola (LP) $\alpha$	$\beta$	-log(Likelihood)	$\Delta\log(\text{Likelihood})$
pre-flare	1.10 ± 0.07	2.42 ± 0.08	0.08 ± 0.05	33108.8	-1.3
flare	5.05 ± 0.15	2.30 ± 0.04	0.11 ± 0.03	36260.6	-10.6
post-flare	2.48 ± 0.09	2.21 ± 0.05	0.09 ± 0.03	49187.9	-6.5
Activity	$F_{0.1-300 \text{ GeV}}$ ( $10^{-6} \text{ ph cm}^{-2} \text{ s}^{-1}$ )	PLExCutoff (PLEC) $\Gamma_{PLEC}$	$E_{cutoff}$ [GeV]	-log(Likelihood)	$\Delta\log(\text{Likelihood})$
pre-flare	1.10 ± 0.07	2.37 ± 0.10	5.948 ± 4.510	33108.5	-1.6
flare	5.10 ± 0.15	2.27 ± 0.05	5.740 ± 1.830	36262.9	-8.3
post-flare	2.52 ± 0.09	2.24 ± 0.05	11.670± 5.692	49191.0	-3.4

**Table 9**

All the columns represent the same parameters as mentioned in Table-7, here results are shown for flare-2(A)

PowerLaw (PL)					
Activity	$F_{0.1-300 \text{ GeV}}$ ( $10^{-6} \text{ ph cm}^{-2} \text{ s}^{-1}$ )	$\Gamma$		$-\log(\text{Likelihood})$	
pre-flare	$0.40 \pm 0.07$	$2.22 \pm 0.13$	-	14835.3	-
flare(I)	$2.80 \pm 0.20$	$2.19 \pm 0.06$	-	9462.8	-
plateau	$2.12 \pm 0.21$	$2.32 \pm 0.09$	-	6705.2	-
flare(II)	$2.89 \pm 0.14$	$2.21 \pm 0.04$	-	21374.7	-
post-flare	$0.56 \pm 0.08$	$2.23 \pm 0.10$	-	15417.3	-
LogParabola (LP)					
Activity	$F_{0.1-300 \text{ GeV}}$ ( $10^{-6} \text{ ph cm}^{-2} \text{ s}^{-1}$ )	$\alpha$	$\beta$	$\log(\text{Likelihood})$	$\Delta\log(\text{Likelihood})$
pre-flare	$0.39 \pm 0.07$	$2.13 \pm 0.21$	$0.04 \pm 0.08$	14835.1	-0.2
flare(I)	$2.68 \pm 0.21$	$2.06 \pm 0.10$	$0.07 \pm 0.05$	9461.2	-1.6
plateau	$1.79 \pm 0.21$	$2.07 \pm 0.15$	$0.10 \pm 0.07$	6697.8	-7.4
flare(II)	$2.65 \pm 0.14$	$1.95 \pm 0.07$	$0.17 \pm 0.04$	21362.3	-12.4
post-flare	$0.50 \pm 0.08$	$1.97 \pm 0.21$	$0.14 \pm 0.10$	15416.0	-1.3
PLExpCutoff (PLEC)					
Activity	$F_{0.1-300 \text{ GeV}}$ ( $10^{-6} \text{ ph cm}^{-2} \text{ s}^{-1}$ )	$\Gamma_{PLEC}$	$E_{cutoff}$ [GeV]	$-\log(\text{Likelihood})$	$\Delta\log(\text{Likelihood})$
pre-flare	$0.38 \pm 0.07$	$2.08 \pm 0.22$	$9.546 \pm 12.560$	14834.6	-0.7
flare(I)	$2.71 \pm 0.20$	$2.07 \pm 0.10$	$11.270 \pm 8.127$	9461.0	-1.8
plateau	$1.80 \pm 0.21$	$2.03 \pm 0.16$	$5.316 \pm 4.204$	6697.3	-7.9
flare(II)	$2.69 \pm 0.14$	$1.86 \pm 0.09$	$2.699 \pm 0.733$	21359.9	-14.8
post-flare	$0.51 \pm 0.08$	$1.94 \pm 0.21$	$4.121 \pm 3.184$	15415.7	-1.6

**Table 10**

All the columns represent the same parameters as mentioned in Table-7, here results are shown for flare-2(B)

PowerLaw (PL)					
Activity	$F_{0.1-300 \text{ GeV}}$ ( $10^{-6} \text{ ph cm}^{-2} \text{ s}^{-1}$ )	$\Gamma$		$-\log(\text{Likelihood})$	
pre-flare	$1.07 \pm 0.10$	$2.38 \pm 0.08$	-	17894.3	-
flare	$2.15 \pm 0.11$	$2.17 \pm 0.04$	-	21202.8	-
post-flare	$0.71 \pm 0.07$	$2.57 \pm 0.10$	-	20681.9	-
LogParabola (LP)					
Activity	$F_{0.1-300 \text{ GeV}}$ ( $10^{-6} \text{ ph cm}^{-2} \text{ s}^{-1}$ )	$\alpha$	$\beta$	$-\log(\text{Likelihood})$	$\Delta\log(\text{Likelihood})$
pre-flare	$1.02 \pm 0.11$	$2.26 \pm 0.13$	$0.09 \pm 0.07$	17893.1	-1.2
flare	$2.03 \pm 0.11$	$1.97 \pm 0.07$	$0.13 \pm 0.04$	21196.0	-6.8
post-flare	$0.70 \pm 0.07$	$2.48 \pm 0.13$	$0.11 \pm 0.10$	20681.2	-0.7
PLExpCutoff (PLEC)					
Activity	$F_{0.1-300 \text{ GeV}}$ ( $10^{-6} \text{ ph cm}^{-2} \text{ s}^{-1}$ )	$\Gamma_{PLEC}$	$E_{cutoff}$ [GeV]	$-\log(\text{Likelihood})$	$\Delta\log(\text{Likelihood})$
pre-flare	$1.03 \pm 0.10$	$2.23 \pm 0.15$	$6.094 \pm 5.426$	17893.1	-1.2
flare	$2.06 \pm 0.11$	$1.98 \pm 0.08$	$5.818 \pm 2.364$	21196.6	-6.2
post-flare	$0.70 \pm 0.07$	$2.46 \pm 0.17$	$6.339 \pm 8.688$	20681.5	-0.4

**Table 11**

All the columns represent the same parameters as mentioned in Table-7, here results are shown for flare-2(C)

PowerLaw (PL)					
Activity	$F_{0.1-300 \text{ GeV}}$ ( $10^{-6} \text{ ph cm}^{-2} \text{ s}^{-1}$ )	$\Gamma$		$-\log(\text{Likelihood})$	
pre-flare	$2.55 \pm 0.17$	$2.44 \pm 0.06$	-	13635.9	-
flare	$9.16 \pm 0.30$	$2.13 \pm 0.03$	-	17028.5	-
post-flare	$2.25 \pm 0.17$	$2.30 \pm 0.07$	-	11397.9	-
LogParabola (LP)					
Activity	$F_{0.1-300 \text{ GeV}}$ ( $10^{-6} \text{ ph cm}^{-2} \text{ s}^{-1}$ )	$\alpha$	$\beta$	$-\log(\text{Likelihood})$	$\Delta\log(\text{Likelihood})$
pre-flare	$2.70 \pm 0.17$	$2.45 \pm 0.08$	$0.051 \pm 0.050$	13642.8	6.9
flare	$8.92 \pm 0.30$	$2.03 \pm 0.04$	$0.06 \pm 0.02$	17023.4	-5.1
post-flare	$2.25 \pm 0.17$	$2.30 \pm 0.07$	$0.00 \pm 0.00$	11397.9	0.0
PLExpCutoff (PLEC)					
Activity	$F_{0.1-300 \text{ GeV}}$ ( $10^{-6} \text{ ph cm}^{-2} \text{ s}^{-1}$ )	$\Gamma_{PLEC}$	$E_{cutoff}$ [GeV]	$-\log(\text{Likelihood})$	$\Delta\log(\text{Likelihood})$
pre-flare	$2.50 \pm 0.17$	$2.34 \pm 0.10$	$9.067 \pm 8.024$	13634.8	-1.1
flare	$9.00 \pm 0.31$	$2.05 \pm 0.04$	$18.030 \pm 7.530$	17023.2	-5.3
post-flare	$2.22 \pm 0.17$	$2.26 \pm 0.07$	$30.000 \pm 0.080$	11398.6	0.7



**Table 12**

All the columns represent the same parameters as mentioned in Table-7, here results are shown for flare-2(D)

PowerLaw (PL)					
Activity	$F_{0.1-300 \text{ GeV}}$ ( $10^{-6} \text{ ph cm}^{-2} \text{ s}^{-1}$ )	$\Gamma$		$-\log(\text{Likelihood})$	
pre-flare	1.45±0.12	2.65±0.10	-	14564.0	-
flare	5.55±0.13	2.24±0.02	-	59688.8	-
post-flare	1.65±0.07	2.48±0.04	-	47148.3	-
LogParabola (LP)					
Activity	$F_{0.1-300 \text{ GeV}}$ ( $10^{-6} \text{ ph cm}^{-2} \text{ s}^{-1}$ )	$\alpha$	$\beta$	$-\log(\text{Likelihood})$	$\Delta\log(\text{Likelihood})$
pre-flare	1.41±0.13	2.55±0.12	0.14±0.10	14562.7	-1.3
flare	5.35±0.13	2.11±0.03	0.09±0.02	59672.5	-16.3
post-flare	1.63±0.07	2.42±0.05	0.05±0.03	47147.0	-1.3
PLExpCutoff (PLEC)					
Activity	$F_{0.1-300 \text{ GeV}}$ ( $10^{-6} \text{ ph cm}^{-2} \text{ s}^{-1}$ )	$\Gamma_{PLEC}$	$E_{cutoff}$ [GeV]	$-\log(\text{Likelihood})$	$\Delta\log(\text{Likelihood})$
pre-flare	1.42±0.13	2.44±0.18	3.140±2.743	14562.9	-1.9
flare	5.44±0.13	2.14±0.03	12.310±3.515	59677.4	-11.4
post-flare	1.63±0.07	2.38±0.07	8.401±5.696	47146.2	-2.1

**Table 13**

All the columns represent the same parameters as mentioned in Table-7, here results are shown for flare-2(E)

PowerLaw (PL)					
Activity	$F_{0.1-300 \text{ GeV}}$ ( $10^{-6} \text{ ph cm}^{-2} \text{ s}^{-1}$ )	$\Gamma$		$-\log(\text{Likelihood})$	
pre-flare	2.91±0.09	2.40±0.03	-	49012.7	-
flare(I)	4.94±0.09	2.29±0.02	-	70122.5	-
flare(II)	4.13±0.13	2.49±0.03	-	26676.5	-
post-flare	1.26±1.05	2.64±0.08	-	13838.9	-
LogParabola (LP)					
Activity	$F_{0.1-300 \text{ GeV}}$ ( $10^{-6} \text{ ph cm}^{-2} \text{ s}^{-1}$ )	$\alpha$	$\beta$	$-\log(\text{Likelihood})$	$\Delta\log(\text{Likelihood})$
pre-flare	2.87±0.10	2.36±0.04	0.03±0.02	49011.6	-1.1
flare(I)	4.78±0.09	2.17±0.02	0.09±0.01	70096.3	-26.2
flare(II)	4.06±0.14	2.44±0.04	0.06±0.03	26674.2	-2.3
post-flare	1.24±0.11	2.58±0.11	0.07±0.06	13838.4	-0.5
PLExpCutoff (PLEC)					
Activity	$F_{0.1-300 \text{ GeV}}$ ( $10^{-6} \text{ ph cm}^{-2} \text{ s}^{-1}$ )	$\Gamma_{PLEC}$	$E_{cutoff}$ [GeV]	$-\log(\text{Likelihood})$	$\Delta\log(\text{Likelihood})$
pre-flare	2.89±0.09	2.37±0.03	29.970±3.615	49011.7	-1.0
flare(I)	4.83±0.09	2.16±0.03	7.612±1.533	70099.0	-23.5
flare(II)	4.08±0.14	2.41±0.05	9.709±5.118	26673.7	-2.8
post-flare	1.24±0.11	2.54±0.14	7.244±8.785	13838.4	-0.5

**Table 14**

All the columns represent the same parameters as mentioned in Table-7, here results are shown for Flare-3

PowerLaw (PL)					
Activity	$F_{0.1-300 \text{ GeV}}$ ( $10^{-6} \text{ ph cm}^{-2} \text{ s}^{-1}$ )	$\Gamma$		$-\log(\text{Likelihood})$	
pre-flare	1.28±0.02	2.47±0.01	-	15158.0	-
flare(I)	2.88±0.06	2.32±0.01	-	24129.8	-
flare(II)	2.22±0.01	2.35±0.02	-	29884.4	-
post-flare	1.78±0.02	2.40±0.01	-	30937.3	-
LogParabola (LP)					
Activity	$F_{0.1-300 \text{ GeV}}$ ( $10^{-6} \text{ ph cm}^{-2} \text{ s}^{-1}$ )	$\alpha$	$\beta$	$-\log(\text{Likelihood})$	$\Delta\log(\text{Likelihood})$
pre-flare	1.29±0.11	2.45±0.09	0.02±0.00	15158.0	0.0
flare(I)	2.74±0.08	2.19±0.05	0.10±0.04	24123.9	-5.9
flare(II)	2.17±0.06	2.27±0.03	0.06±0.03	29883.2	-1.2
post-flare	1.76±0.08	2.36±0.04	0.04±0.01	30936.7	-0.6
PLExpCutoff (PLEC)					
Activity	$F_{0.1-300 \text{ GeV}}$ ( $10^{-6} \text{ ph cm}^{-2} \text{ s}^{-1}$ )	$\Gamma_{PLEC}$	$E_{cutoff}$ [GeV]	$\log(\text{Likelihood})$	$\Delta\log(\text{Likelihood})$
pre-flare	1.27±0.10	2.41±0.08	16.580±2.897	15157.1	-0.7
flare(I)	2.78±0.10	2.15±0.05	5.022±0.180	24123.7	-6.1
flare(II)	2.17±0.05	2.24±0.03	9.043±0.223	29881.6	-2.8
post-flare	1.76±0.06	2.35±0.05	18.030±1.724	30936.5	-0.8

**Table 15**

All the columns represent the same parameters as mentioned in Table-7, here results are shown for flare-4(A)

		PowerLaw (PL)			
Activity	$F_{0.1-300 \text{ GeV}}$ ( $10^{-6} \text{ ph cm}^{-2} \text{ s}^{-1}$ )	$\Gamma$		$-\log(\text{Likelihood})$	
pre-flare	$2.21 \pm 0.07$	$2.32 \pm 0.03$	-	50195.9	
flare	$6.41 \pm 0.17$	$2.14 \pm 0.04$	-	30084.0	
post-flare	$2.92 \pm 0.12$	$2.42 \pm 0.04$	-	34033.0	
		LogParabola (LP)			
Activity	$F_{0.1-300 \text{ GeV}}$ ( $10^{-6} \text{ ph cm}^{-2} \text{ s}^{-1}$ )	$\alpha$	$\beta$	$-\log(\text{Likelihood})$	$\Delta\log(\text{Likelihood})$
pre-flare	$2.14 \pm 0.07$	$2.20 \pm 0.04$	$0.09 \pm 0.03$	50188.6	-7.3
flare	$6.03 \pm 0.18$	$2.03 \pm 0.06$	$0.06 \pm 0.03$	30067.9	-16.1
post-flare	$2.83 \pm 0.12$	$2.33 \pm 0.05$	$0.08 \pm 0.03$	34029.4	-3.6
		PLExpCutoff (PLEC)			
Activity	$F_{0.1-300 \text{ GeV}}$ ( $10^{-6} \text{ ph cm}^{-2} \text{ s}^{-1}$ )	$\Gamma_{PLEC}$	$E_{cutoff}$ [GeV]	$-\log(\text{Likelihood})$	$\Delta\log(\text{Likelihood})$
pre-flare	$2.17 \pm 0.07$	$2.21 \pm 0.05$	$9.657 \pm 3.964$	50191.3	-4.6
flare	$6.35 \pm 0.17$	$2.04 \pm 0.07$	$12.785 \pm 8.115$	30080.7	-3.3
post-flare	$2.86 \pm 0.12$	$2.32 \pm 0.06$	$9.118 \pm 5.157$	34030.2	-2.8

**Table 16**

All the column represents the same parameters as mentioned in Table-7, here results are shown for flare-4(B)

		PowerLaw (PL)			
Activity	$F_{0.1-300 \text{ GeV}}$ ( $10^{-6} \text{ ph cm}^{-2} \text{ s}^{-1}$ )	$\Gamma$		$-\log(\text{Likelihood})$	
pre-flare	$1.64 \pm 0.08$	$2.40 \pm 0.05$	-	38092.3	
flare(I)	$4.22 \pm 0.11$	$2.19 \pm 0.04$	-	39757.9	
flare(II)	$3.75 \pm 0.11$	$2.20 \pm 0.04$	-	36387.9	
post-flare	$1.59 \pm 0.12$	$2.39 \pm 0.07$	-	16506.6	
		LogParabola (LP)			
Activity	$F_{0.1-300 \text{ GeV}}$ ( $10^{-6} \text{ ph cm}^{-2} \text{ s}^{-1}$ )	$\alpha$	$\beta$	$-\log(\text{Likelihood})$	$\Delta\log(\text{Likelihood})$
pre-flare	$1.62 \pm 0.08$	$2.37 \pm 0.06$	$0.02 \pm 0.03$	38092.0	-0.3
flare(I)	$4.12 \pm 0.11$	$2.09 \pm 0.05$	$0.07 \pm 0.00$	39749.7	-8.2
flare(II)	$3.61 \pm 0.11$	$2.06 \pm 0.04$	$0.10 \pm 0.02$	36375.6	-12.3
post-flare	$1.49 \pm 0.12$	$2.21 \pm 0.11$	$0.15 \pm 0.07$	16503.3	-3.3
		PLExpCutoff (PLEC)			
Activity	$F_{0.1-300 \text{ GeV}}$ ( $10^{-6} \text{ ph cm}^{-2} \text{ s}^{-1}$ )	$\Gamma_{PLEC}$	$E_{cutoff}$ [GeV]	$-\log(\text{Likelihood})$	$\Delta\log(\text{Likelihood})$
pre-flare	$1.62 \pm 0.08$	$2.36 \pm 0.05$	$30.000 \pm 0.050$	38093.6	1.3
flare(I)	$4.14 \pm 0.11$	$2.06 \pm 0.05$	$9.073 \pm 0.308$	39747.0	-10.9
flare(II)	$3.67 \pm 0.11$	$2.08 \pm 0.04$	$9.743 \pm 3.159$	36378.8	-9.1
post-flare	$1.51 \pm 0.12$	$2.12 \pm 0.14$	$3.060 \pm 1.610$	16503.0	-3.6

**Table 17**

All the columns represent the same parameters as mentioned in Table-7, here results are shown for flare-4(C)

		PowerLaw (PL)			
Activity	$F_{0.1-300 \text{ GeV}}$ ( $10^{-6} \text{ ph cm}^{-2} \text{ s}^{-1}$ )	$\Gamma$		$-\log(\text{Likelihood})$	
pre-flare	$1.15 \pm 0.11$	$2.42 \pm 0.09$	-	15800.4	
flare	$4.89 \pm 0.15$	$1.96 \pm 0.02$	-	30002.9	
post-flare	$1.22 \pm 0.08$	$2.42 \pm 0.06$	-	27063.2	
		LogParabola (LP)			
Activity	$F_{0.1-300 \text{ GeV}}$ ( $10^{-6} \text{ ph cm}^{-2} \text{ s}^{-1}$ )	$\alpha$	$\beta$	$-\log(\text{Likelihood})$	$\Delta\log(\text{Likelihood})$
pre-flare	$1.35 \pm 0.11$	$2.55 \pm 0.09$	$0.00 \pm 0.00$	15817.6	17.2
flare	$4.64 \pm 0.16$	$1.81 \pm 0.04$	$0.06 \pm 0.01$	29993.2	-9.7
post-flare	$1.16 \pm 0.09$	$2.29 \pm 0.10$	$0.11 \pm 0.06$	27061.0	-2.2
		PLExpCutoff (PLEC)			
Activity	$F_{0.1-300 \text{ GeV}}$ ( $10^{-6} \text{ ph cm}^{-2} \text{ s}^{-1}$ )	$\Gamma_{PLEC}$	$E_{cutoff}$ [GeV]	$-\log(\text{Likelihood})$	$\Delta\log(\text{Likelihood})$
pre-flare	$1.12 \pm 0.11$	$2.31 \pm 0.13$	$8.931 \pm 9.809$	15799.8	-0.6
flare	$4.75 \pm 0.16$	$1.88 \pm 0.03$	$29.710 \pm 8.166$	29994.5	-8.4
post-flare	$1.19 \pm 0.09$	$2.29 \pm 0.11$	$7.354 \pm 5.857$	27061.7	-1.5

**Table 18**

All the columns represent the same parameters as mentioned in Table-7, here results are shown for Flare-5

Activity	$F_{0.1-300 \text{ GeV}}$ ( $10^{-6} \text{ ph cm}^{-2} \text{ s}^{-1}$ )	PowerLaw (PL)			
		$\Gamma$		$-\log(\text{Likelihood})$	
pre-flare	$1.64 \pm 0.12$	$2.58 \pm 0.08$	-	14412.7	-
flare	$3.01 \pm 0.11$	$2.39 \pm 0.04$	-	28013.0	-
post-flare	$1.85 \pm 0.09$	$2.38 \pm 0.04$	-	29145.4	-
Activity	$F_{0.1-300 \text{ GeV}}$ ( $10^{-6} \text{ ph cm}^{-2} \text{ s}^{-1}$ )	LogParabola (LP)		$-\log(\text{Likelihood})$	$\Delta \log(\text{Likelihood})$
		$\alpha$	$\beta$		
pre-flare	$1.63 \pm 0.12$	$2.55 \pm 0.10$	$0.04 \pm 0.06$	14412.5	-0.2
flare	$2.93 \pm 0.11$	$2.28 \pm 0.05$	$0.10 \pm 0.03$	28007.3	-5.7
post-flare	$1.82 \pm 0.09$	$2.31 \pm 0.06$	$0.06 \pm 0.04$	29143.9	-1.5
Activity	$F_{0.1-300 \text{ GeV}}$ ( $10^{-6} \text{ ph cm}^{-2} \text{ s}^{-1}$ )	PLExpCutoff (PLEC)		$-\log(\text{Likelihood})$	$\Delta \log(\text{Likelihood})$
		$\Gamma_{PLEC}$	$E_{cutoff}$ [GeV]		
pre-flare	$1.62 \pm 0.12$	$2.44 \pm 0.14$	$4.640 \pm 4.235$	14411.7	-1.0
flare	$2.95 \pm 0.11$	$2.23 \pm 0.07$	$5.016 \pm 2.001$	28007.2	-5.8
post-flare	$1.83 \pm 0.09$	$2.33 \pm 0.06$	$19.040 \pm 17.200$	29144.5	-0.9

**Table 19**

The reduced- $\chi^2$  for SEDs fitted by PowerLaw (PL), LogParabola (LP) and PowerLaw ExpCutoff (PLEC) for the flaring episodes are displayed below. In most cases LP and in a few cases PLEC provide the best fit to the data. Cutoff energies found with PLEC vary from one flare to another, which could be due to different emission regions of these flares

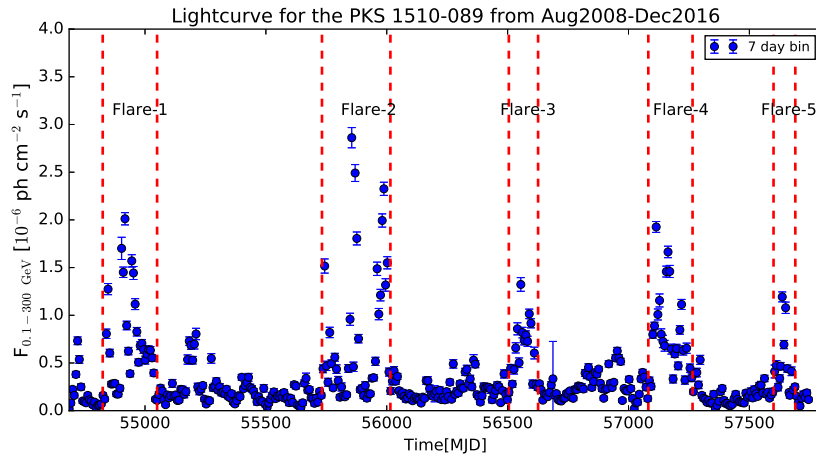
Activity	Reduced- $\chi^2$			$E_{cutoff}$ for PLEC (GeV)
	PL	LP	PLEC	
flare-1(A)				
flare(I)	2.28	2.31	1.98	$30.00 \pm 0.25$
flare(II)	2.90	0.12	1.09	$15.98 \pm 6.36$
flare-1(B)				
flare	5.06	0.58	1.03	$5.74 \pm 1.83$
flare-2(A)				
flare(I)	3.66	1.91	2.40	$11.27 \pm 8.13$
flare(II)	2.84	0.92	0.48	$2.70 \pm 0.73$
flare-2(B)				
flare	2.15	0.23	0.43	$5.82 \pm 2.36$
flare-2(C)				
flare	1.73	0.41	0.83	$18.03 \pm 7.53$
flare-2(D)				
flare	8.14	0.43	2.83	$12.31 \pm 3.51$
flare-2(E)				
flare(I)	10.23	1.63	2.41	$7.61 \pm 1.53$
flare(II)	0.43	0.15	0.06	$9.71 \pm 5.12$
Flare-3				
flare(I)	2.73	0.91	1.19	$5.02 \pm 0.18$
flare(II)	0.41	0.42	0.34	$9.04 \pm 0.22$
flare-4(A)				
flare	11.93	3.25	5.82	$12.78 \pm 8.11$
flare-4(B)				
flare(I)	2.41	2.95	1.78	$9.07 \pm 0.31$
flare(II)	8.60	0.50	3.30	$9.74 \pm 3.16$
flare-4(C)				
flare	4.41	1.00	1.84	$29.71 \pm 8.16$
Flare-5				
flare	1.55	0.43	0.50	$5.01 \pm 2.00$

**Table 20**

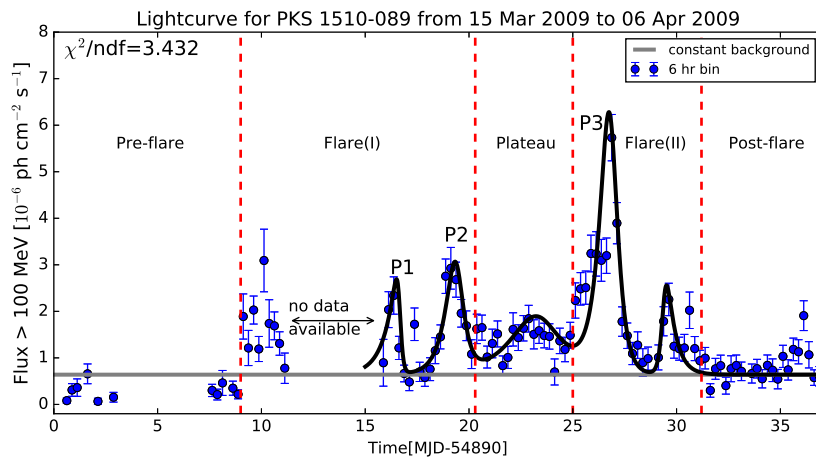
Details of fastest variability time scale of PKS 1510-089 for the whole 8 years data has been presented here. Data which has a significance of at least  $5\sigma$  has been considered (see text for details). Here  $t_{var}$  represents the observed characteristic time scale and  $\Delta t_{var} = t_{var} (1+z)^{-1}$ . R (rise) and D(decay) represent the behavior of the flux in a particular time interval

$T_{start}(t_1)$ (MJD)	$T_{stop}(t_2)$ (MJD)	Flux start ( $F_1$ ) ( $10^{-6}$ ph cm $^{-2}$ s $^{-1}$ )	Flux stop ( $F_2$ ) ( $10^{-6}$ ph cm $^{-2}$ s $^{-1}$ )	$t_{var}$ (hr)	$\Delta t_{var}$ (hr)	Rise/Decay
flare-1(A)						
54916.563	54916.688	1.95±0.45	4.25±0.59	2.67±0.32	1.96±0.17	R
54917.188	54917.313	4.55±0.68	1.75±0.43	-2.18±0.22	-1.60±0.12	D
54917.938	54918.063	0.69±0.25	1.40±0.43	2.96±0.23	2.17±0.12	R
flare-1(B)						
54945.438	54945.563	0.72±0.29	3.09±0.53	1.43±0.22	1.05±0.12	R
54948.938	54949.063	2.25±0.68	5.49±1.91	2.34±0.12	1.72±0.07	R
54949.688	54949.813	3.10±0.55	1.37±0.36	-2.56±0.26	-1.88±0.14	D
flare-2(A)						
55739.313	55739.438	0.89±0.36	2.31±0.52	2.17±0.42	1.59±0.22	R
55745.563	55745.688	3.03±0.63	0.95±0.32	-1.79±0.20	-1.32±0.11	D
55745.688	55745.813	0.95±0.32	1.87±0.70	3.07±0.15	2.26±0.08	R
55746.063	55746.188	6.10±1.50	2.95±0.66	-2.88±0.09	-2.12±0.05	D
55746.438	55746.563	7.01±0.95	3.48±0.66	-2.98±0.23	-2.19±0.12	D
55746.563	55746.688	3.48±0.66	1.19±0.43	-1.94±0.31	-1.42±0.17	D
flare-2(B)						
55767.063	55767.188	1.11±0.45	2.98±0.62	2.11±0.42	1.55±0.23	R
55767.813	55767.938	4.35±1.15	1.94±0.60	-2.59±0.14	-1.90±0.08	D
flare-2(C)						
55852.063	55852.188	5.80±0.84	1.17±0.43	-1.30±0.18	-0.95±0.10	D
55852.313	55852.438	0.91±0.37	2.57±0.87	2.00±0.13	1.47±0.07	R
55852.438	55852.563	2.57±0.87	5.84±1.75	2.53±0.13	1.86±0.07	R
55853.063	55853.188	3.11±0.65	6.28±0.87	2.97±0.30	2.18±0.16	R
55853.188	55853.313	6.28±0.87	3.00±0.60	-2.81±0.24	-2.07±0.13	D
55853.563	55853.688	3.46±1.43	7.20±2.54	2.84±0.24	2.09±0.13	R
55853.688	55853.813	7.20±2.54	25.50±2.34	1.64±0.34	1.21±0.18	R
55853.938	55854.063	13.35±1.27	4.94±0.76	-2.09±0.12	-1.54±0.07	D
flare-2(D)						
55867.313	55867.438	3.49±0.70	1.38±0.59	-2.24±0.54	-1.64±0.29	D
55868.438	55868.563	6.92±1.09	2.74±1.15	-2.25±0.64	-1.65±0.35	D
55868.688	55868.813	1.62±0.72	3.55±0.74	2.66±0.81	1.95±0.43	R
55869.063	55869.188	4.78±0.81	2.19±0.52	-2.67±0.24	-1.96±0.13	D
55869.188	55869.313	2.19±0.52	4.50±0.77	2.89±0.27	2.12±0.15	R
55870.313	55870.438	2.05±0.58	4.10±0.90	3.00±0.28	2.20±0.15	R
55872.563	55872.688	2.66±0.87	6.11±0.86	2.50±0.56	1.84±0.30	R
flare-2(E)						
55989.188	55989.313	3.54±0.59	1.15±0.39	-1.84±0.28	-1.35±0.15	D
55989.313	55989.438	1.15±0.39	2.77±0.56	2.36±0.36	1.74±0.20	R
55990.063	55990.188	1.35±0.38	2.67±0.53	3.06±0.36	2.25±0.20	R
55990.438	55990.563	1.94±0.54	4.33±0.78	2.59±0.32	1.90±0.17	R
55991.313	55991.438	1.01±0.43	2.07±0.50	2.89±0.73	2.12±0.40	R
55991.813	55991.938	1.82±0.43	0.84±0.32	-2.68±0.50	-1.97±0.27	D
55998.938	55999.063	0.78±0.30	1.80±0.54	2.49±0.26	1.83±0.14	R
56000.188	56000.313	1.25±0.41	0.63±0.27	-3.04±0.44	-2.23±0.24	D
56000.688	56000.813	1.35±0.37	2.75±0.52	2.94±0.35	2.16±0.19	R
56001.063	56001.188	2.12±0.45	1.07±0.39	-3.03±0.61	-2.23±0.33	D
Flare-3						
56556.188	56556.313	1.61±0.49	3.88±0.66	2.37±0.36	1.74±0.19	R
56563.313	56563.438	2.05±0.52	0.93±0.39	-1.98±0.38	-1.45±0.21	D
56568.063	56568.188	2.10±0.49	0.99±0.35	-2.76±0.53	-2.03±0.29	D
flare-4(A)						
57113.188	57113.313	0.30±0.13	0.93±0.33	1.84±0.15	1.35±0.08	R
57116.938	57117.063	3.65±0.49	1.73±0.42	-2.78±0.40	-2.04±0.22	D
flare-4(B)						
57164.063	57164.188	1.40±0.38	0.63±0.29	-2.61±0.62	-1.92±0.34	D
57165.688	57165.813	0.97±0.34	2.06±0.47	2.78±0.44	2.04±0.24	R
57166.188	57166.313	1.30±0.46	2.85±0.61	2.66±0.48	1.95±0.26	R
57166.438	57166.563	2.43±0.51	0.98±0.36	-2.29±0.40	-1.68±0.21	D
57166.688	57166.813	1.27±0.41	3.05±0.67	2.38±0.29	1.75±0.16	R
57169.688	57169.813	1.15±0.40	2.21±0.52	3.19±0.58	2.34±0.31	R
57170.438	57170.563	3.61±0.69	0.81±0.34	-1.39±0.21	-1.02±0.11	D
flare-4(C)						
57243.438	57243.563	0.57±0.25	1.98±0.60	1.67±0.19	1.23±0.10	R
57245.813	57245.938	4.60±1.55	2.37±0.94	-3.14±0.29	-2.31±0.16	D
57249.563	57249.688	0.78±0.32	1.94±0.66	2.27±0.18	1.67±0.10	R
Flare-5						
57632.563	57632.688	1.03±0.37	2.09±0.54	2.00±0.33	1.47±0.18	R
57634.938	57635.063	2.30±0.50	1.06±0.35	-2.68±0.39	-1.97±0.21	D
57635.063	57635.188	1.06±0.35	2.13±0.49	2.98±0.43	2.19±0.23	R
57635.188	57635.313	2.13±0.49	0.80±0.30	-2.12±0.31	-1.56±0.17	D

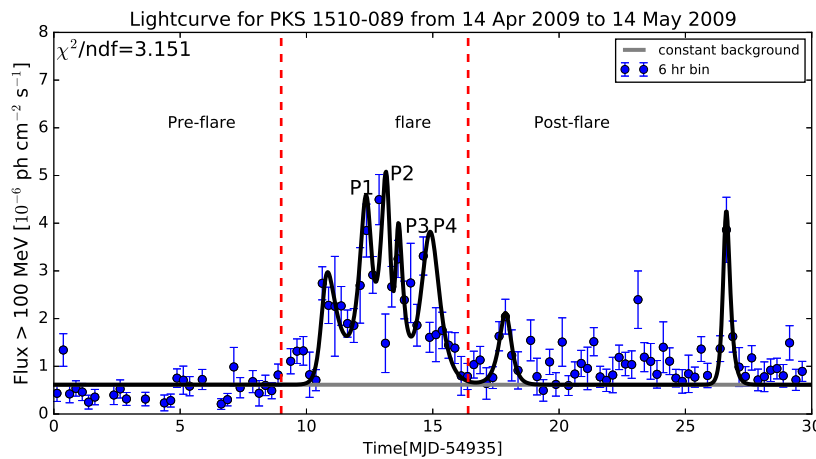




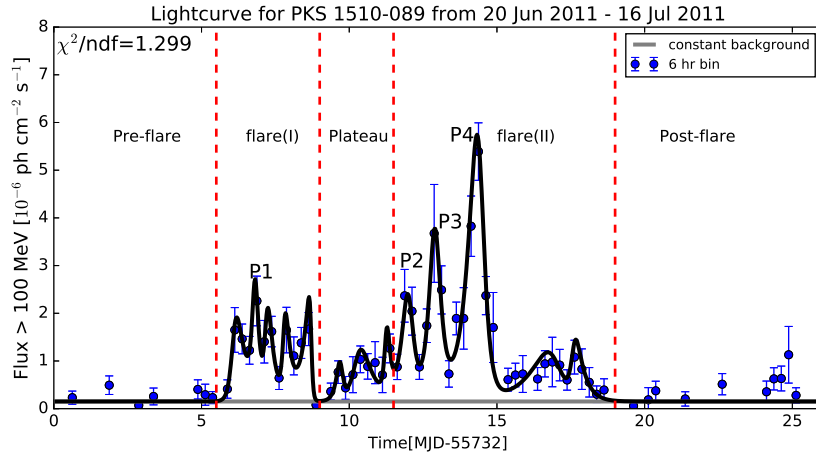
**Figure 1.** Light curve history of the PKS 1510-089. Five flare episodes have been identified and further studied. Their time durations are the following: MJD 54825–55050, MJD 55732–56015, MJD 56505–56626, MJD 57082–57265 and MJD 57657–57753, which are shown by broken red lines.



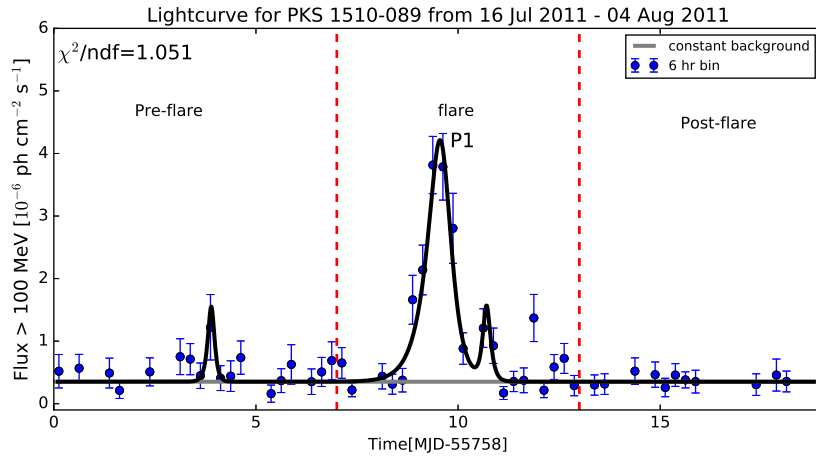
**Figure 2.** Light curve for the flare-1(A) fitted by the sum of exponentials (see text for details). The fitted parameters are given in Table-1. All the different periods of activity have been separated by broken red lines and the light grey line represents the constant state/flux.



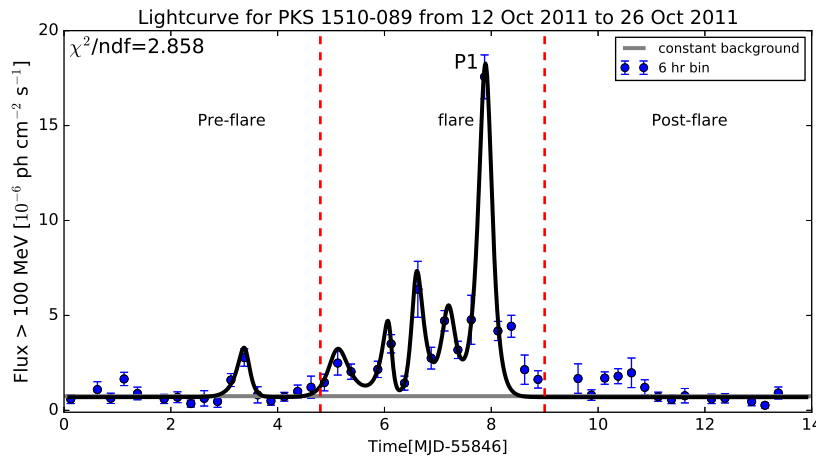
**Figure 3.** Light curve for the flare-1(B) fitted by the sum of exponentials (see text for details). The fitted parameters are given in Table-1. All the different periods of activity have been separated by broken red lines and the light grey line represents the constant state/flux.



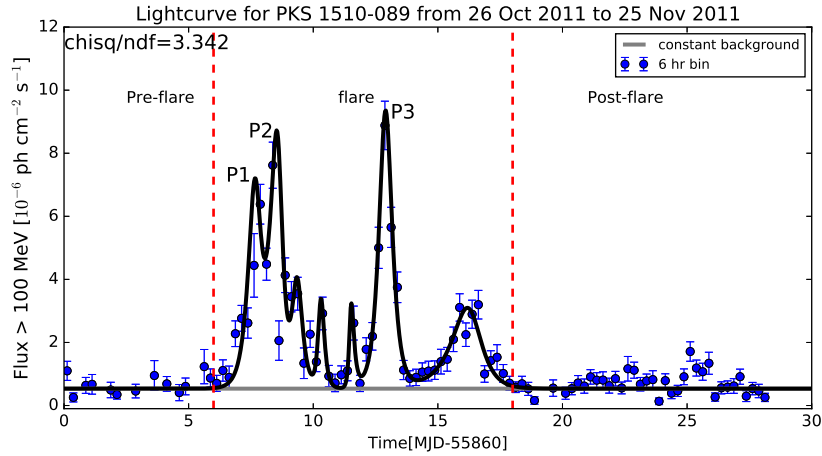
**Figure 4.** Light curve for the flare-2(A) fitted by the sum of exponentials (see text for details). The fitted parameters are given in Table-2. All the different periods of activity have been separated by broken red lines and the light grey line represents the constant state/flux.



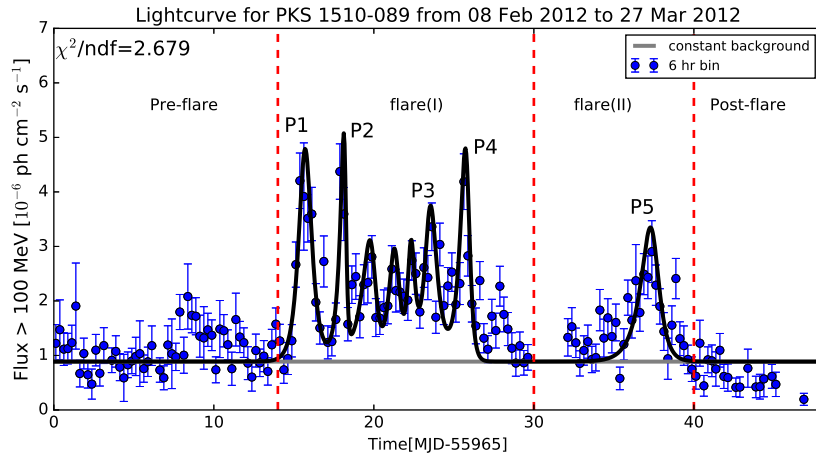
**Figure 5.** Light curve for the flare-2(B) fitted by the sum of exponentials (see text for details). The fitted parameters are given in Table-2. All the different periods of activity have been separated by broken red lines and the light grey line represents the constant state/flux.



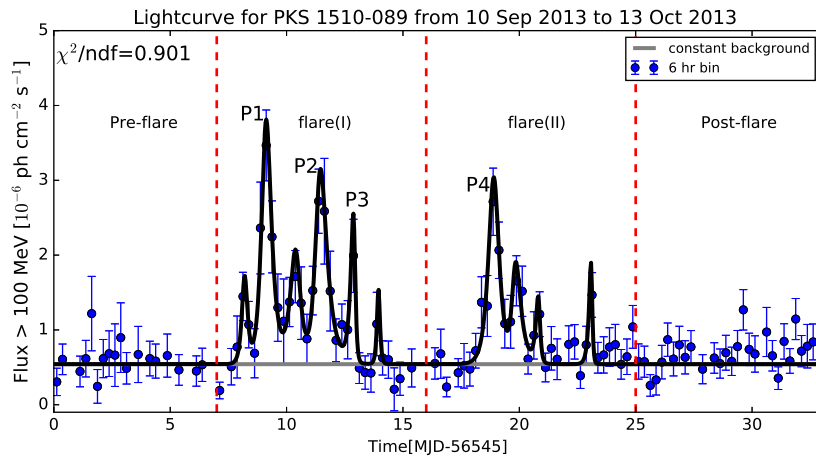
**Figure 6.** Light curve for the flare-2(C) fitted by the sum of exponentials (see text for details). The fitted parameters are given in Table-2. All the different periods of activity have been separated by broken red lines and the light grey line represents the constant state/flux.



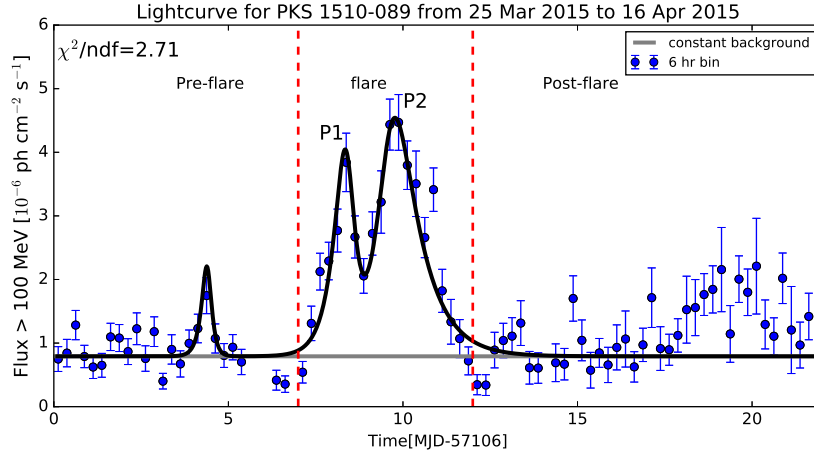
**Figure 7.** Light curve for the flare-2(D) fitted by the sum of exponentials (see text for details). The fitted parameters are given in Table-2. All the different periods of activity have been separated by broken red lines and the light grey line represents the constant state/flux.



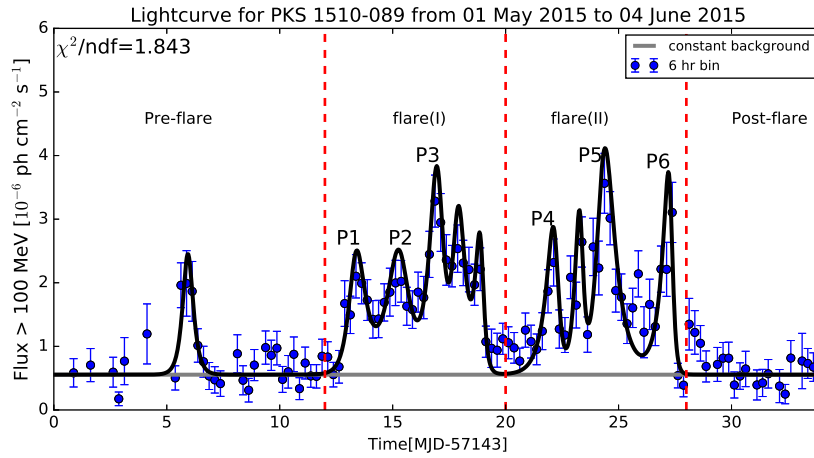
**Figure 8.** Light curve for the flare-2(E) fitted by the sum of exponentials (see text for details). The fitted parameters are given in Table-2. All the different periods of activity have been separated by broken red lines and the light grey line represents the constant state/flux.



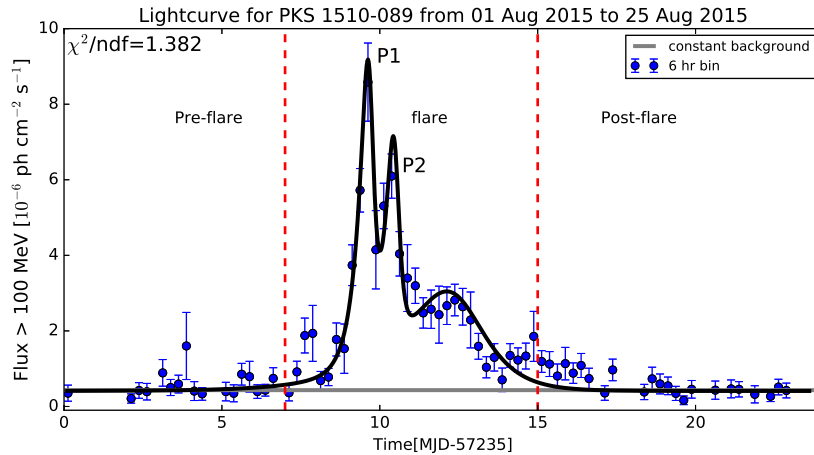
**Figure 9.** Light curve for the flare-3 fitted by the sum of exponentials (see text for details). The fitted parameters are given in Table-3. All the different periods of activity have been separated by broken red lines and the light grey line represents the constant state/flux.



**Figure 10.** Light curve for the flare-4(A) fitted by the sum of exponentials (see text for details). The fitted parameters are given in Table-4. All the different periods of activity have been separated by broken red lines and the light grey line represents the constant state/flux.

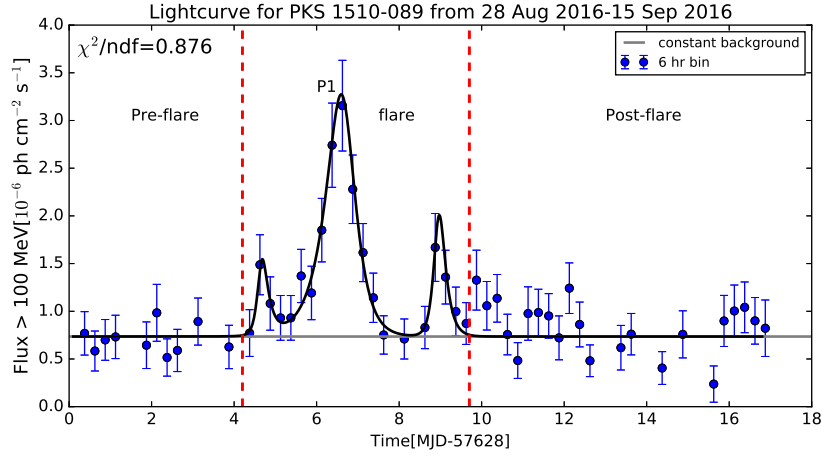


**Figure 11.** Light curve for the flare-4(B) fitted by the sum of exponentials (see text for details). The fitted parameters are given in Table-4. All the different periods of activity have been separated by broken red lines and the light grey line represents the constant state/flux.

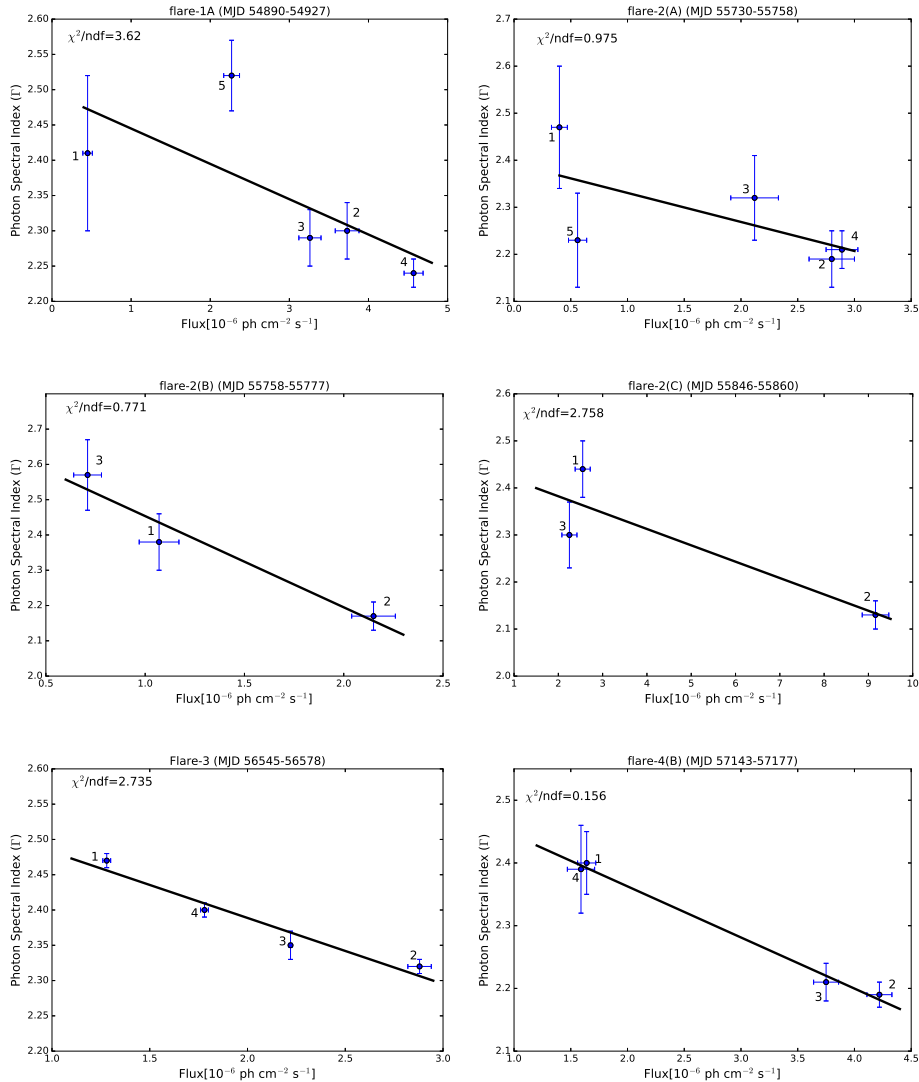


**Figure 12.** Light curve for the flare-4(C) fitted by the sum of exponentials (see text for details). The fitted parameters are given in Table-4. All the different periods of activity have been separated by broken red lines and the light grey line represents the constant state/flux.

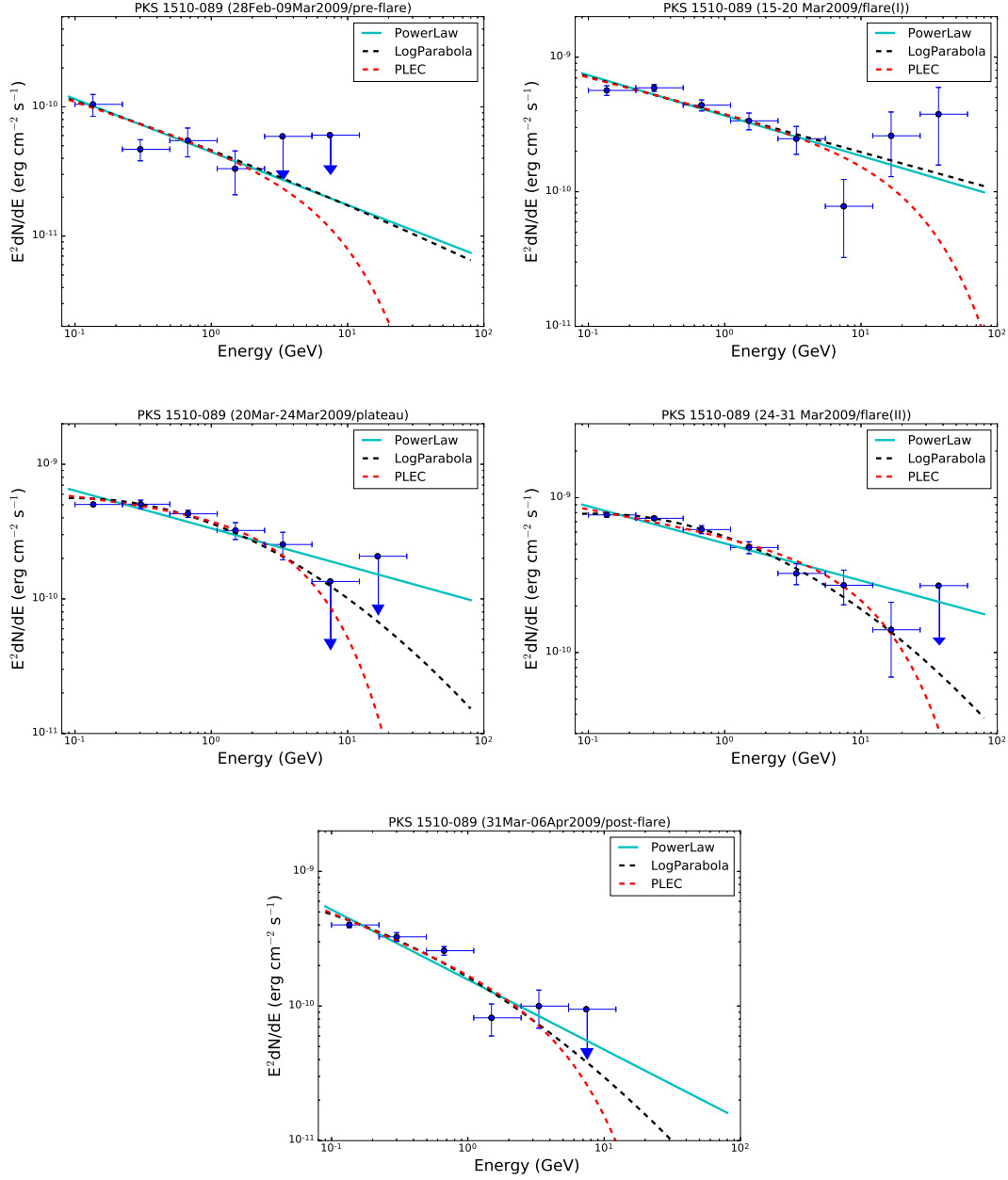




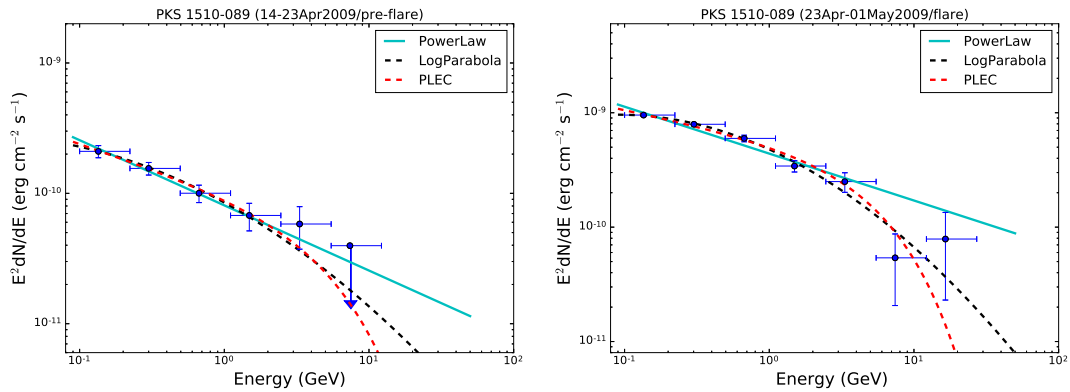
**Figure 13.** Light curve for the flare-5 fitted by the sum of exponentials (see text for details). The fitted parameters are given in Table-5. All the different periods of activity have been separated by broken red lines and the light grey line represents the constant state/flux.



**Figure 14.** Photon index vs flux are plotted for few sub-flares. And the numbers 1, 2, 3, 4, 5 represent the different time periods. Top panel: 1, 2, 3, 4 and 5 represents the pre-flare, flare(I), plateau, flare(II) and post-flare states respectively. Middle panel: 1, 2 and 3 represents the pre-flare, flare and post-flare respectively. Bottom panel: 1, 2, 3, and 4 represents the pre-flare, flare(I), flare(II) and post-flare respectively. All the points have been fitted by the PL spectral type and the corresponding reduced  $\chi^2$  have been mention in the plots. Errors, associated with each data points, are statistical only.



**Figure 15.** Fermi-LAT SEDs during different activity states of flare-1(A) as defined in Fig.2 . PL, LP, PLEC models are shown in cyan, black and red color and their respective parameters are given in the Table-7.



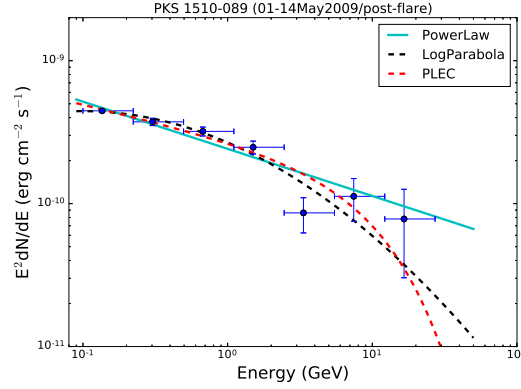


**Figure 16.** Fermi-LAT SEDs during different activity states of flare-1(B) as defined in Fig.3 . PL, LP, PLEC models are shown in cyan, black and red color and there respective parameters are given in the Table-8.

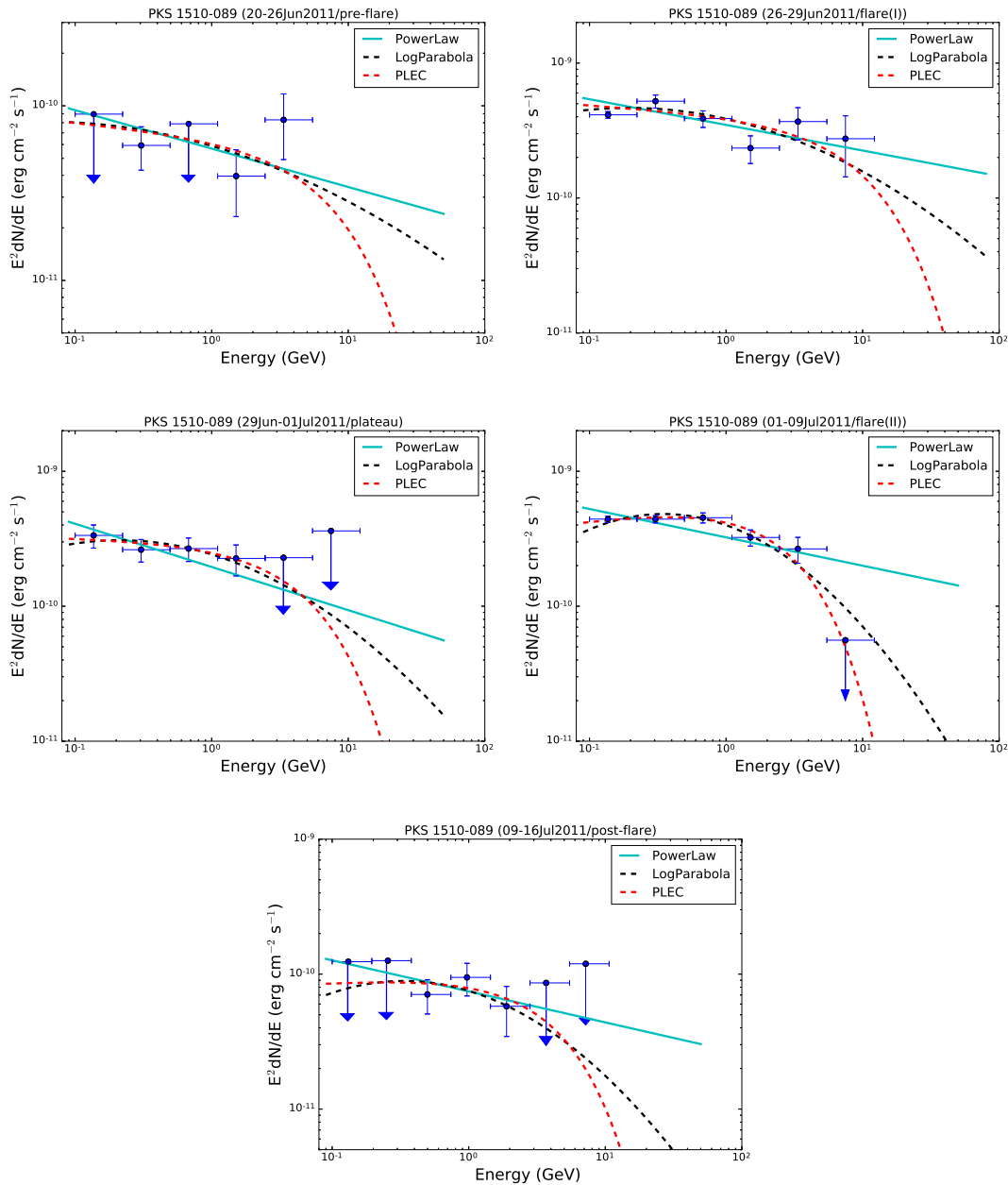


**Figure 17.** Fermi-LAT SEDs during different activity states of flare-2(A) as defined in Fig.4 . PL, LP, PLEC models are shown in cyan, black and red color and there respective parameters are given in the Table-9.

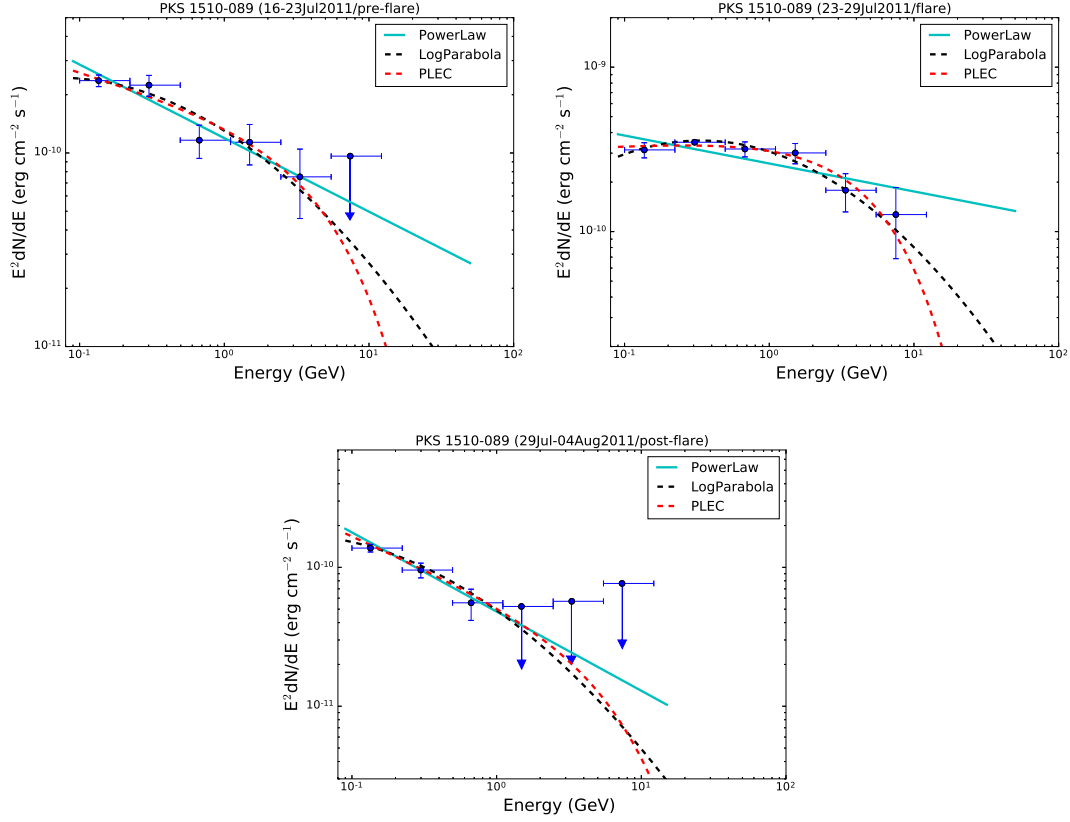


**Figure 18.** Fermi-LAT SEDs during different activity states of flare-2(B) as defined in Fig.5 . PL, LP, PLEC models are shown in cyan, black and red color and there respective parameters are given in the Table-10.

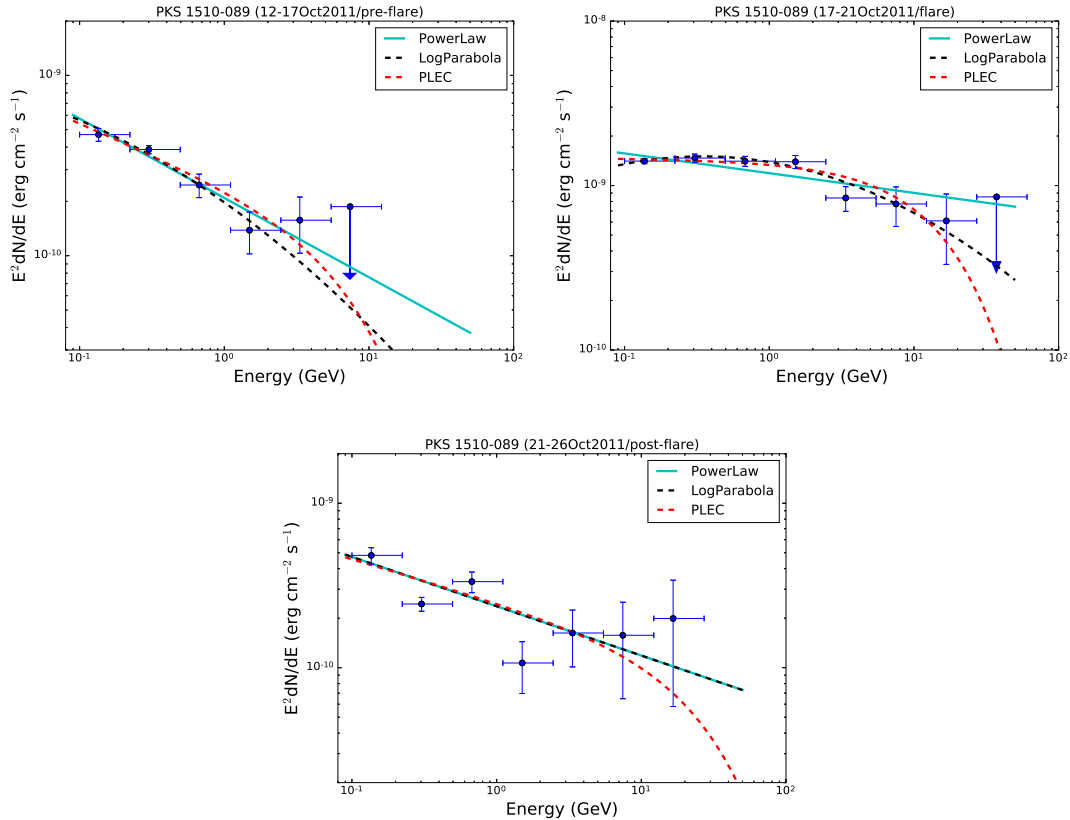


**Figure 19.** Fermi-LAT SEDs during different activity states of flare-2(C) as defined in Fig.6 . PL, LP, PLEC models are shown in cyan, black and red color and there respective parameters are given in the Table-11.

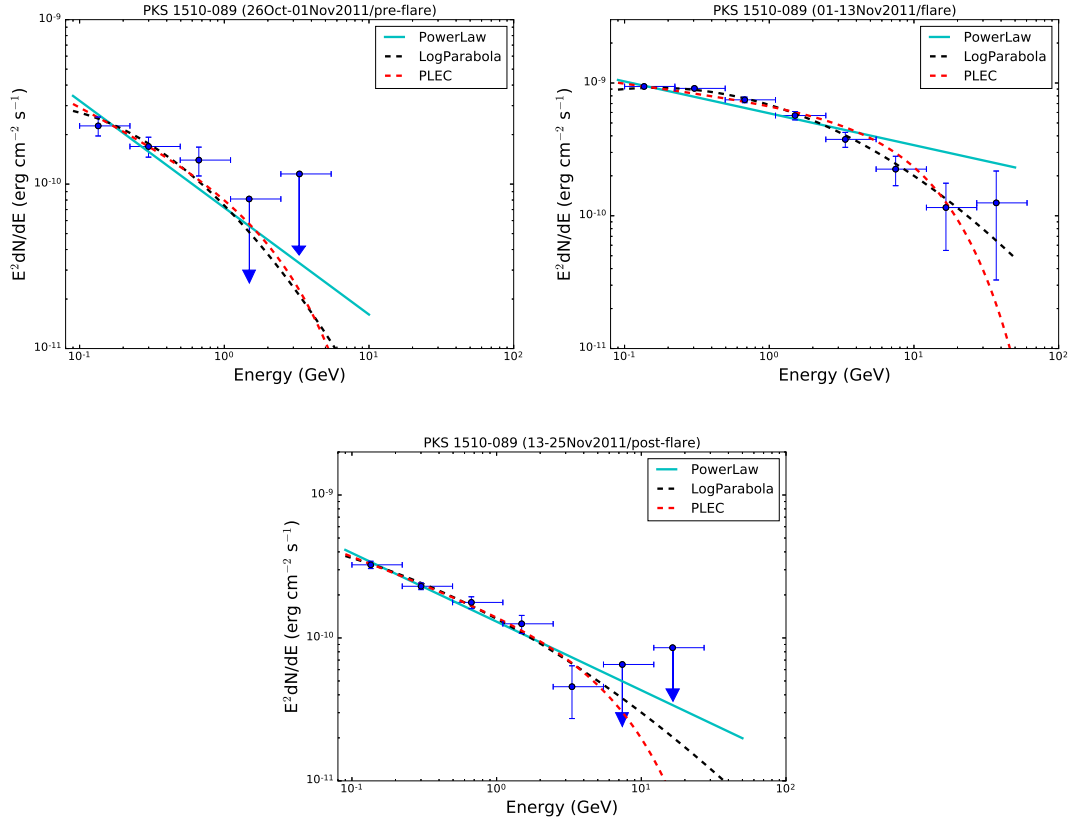


**Figure 20.** Fermi-LAT SEDs during different activity states of flare-2(D) as defined in Fig.7 . PL, LP, PLEC models are shown in cyan, black and red color and there respective parameters are given in the Table-12.

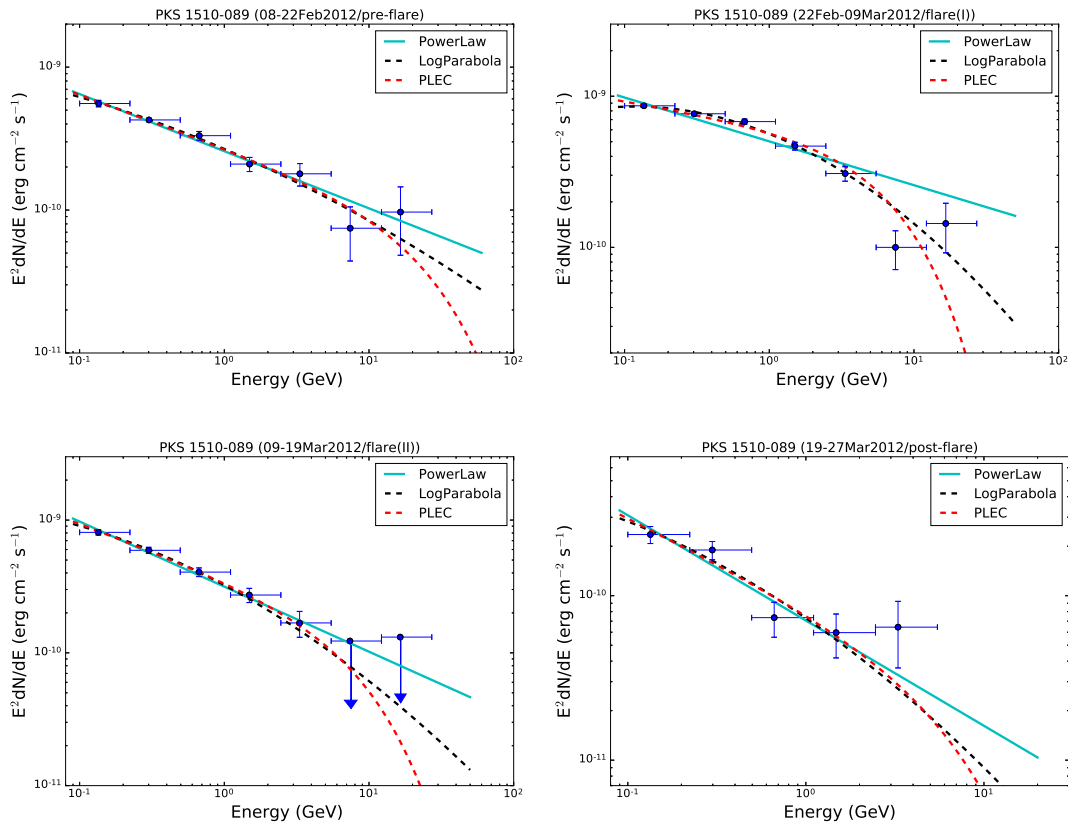


**Figure 21.** Fermi-LAT SEDs during different activity states of flare-2(E) as defined in Fig.8 . PL, LP, PLEC models are shown in cyan, black and red color and there respective parameters are given in the Table-13.

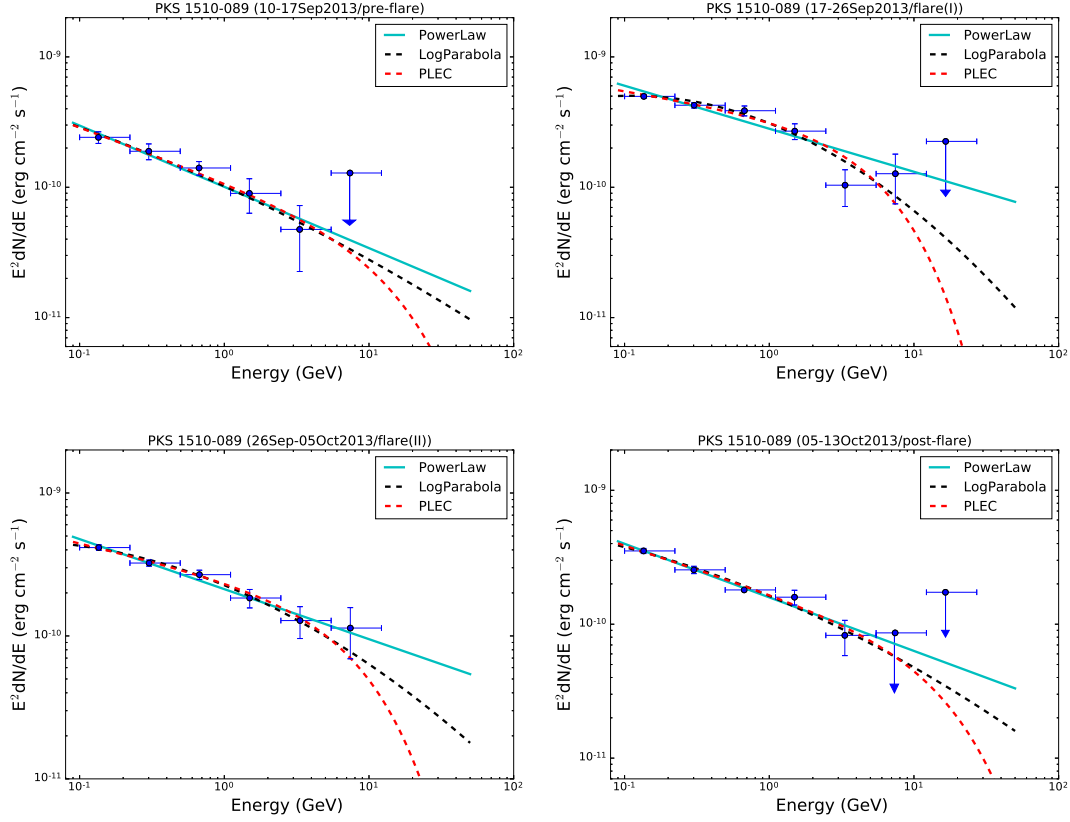


**Figure 22.** Fermi-LAT SEDs during different activity states of Flare-3 as defined in Fig.9 . PL, LP, PLEC models are shown in cyan, black and red color and there respective parameters are given in the Table-14.

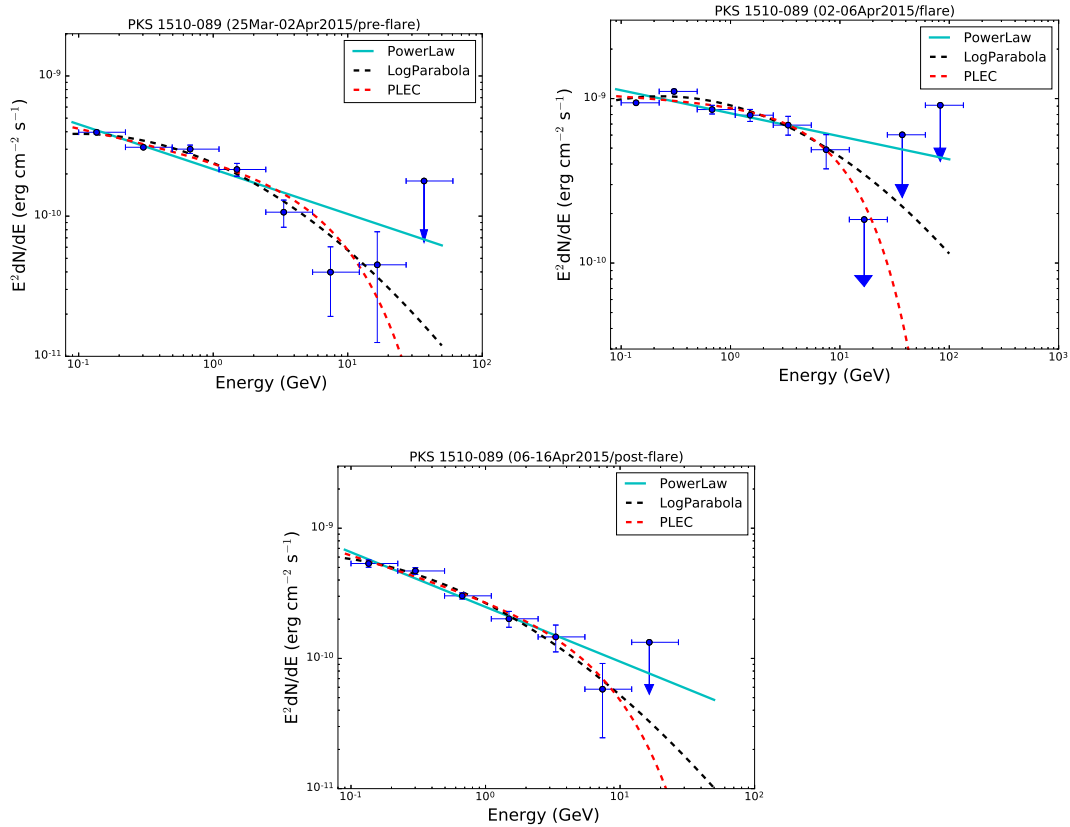


**Figure 23.** Fermi-LAT SEDs during different activity states of flare-4(A) as defined in Fig.10 . PL, LP, PLEC models are shown in cyan, black and red color and there respective parameters are given in the Table-15.



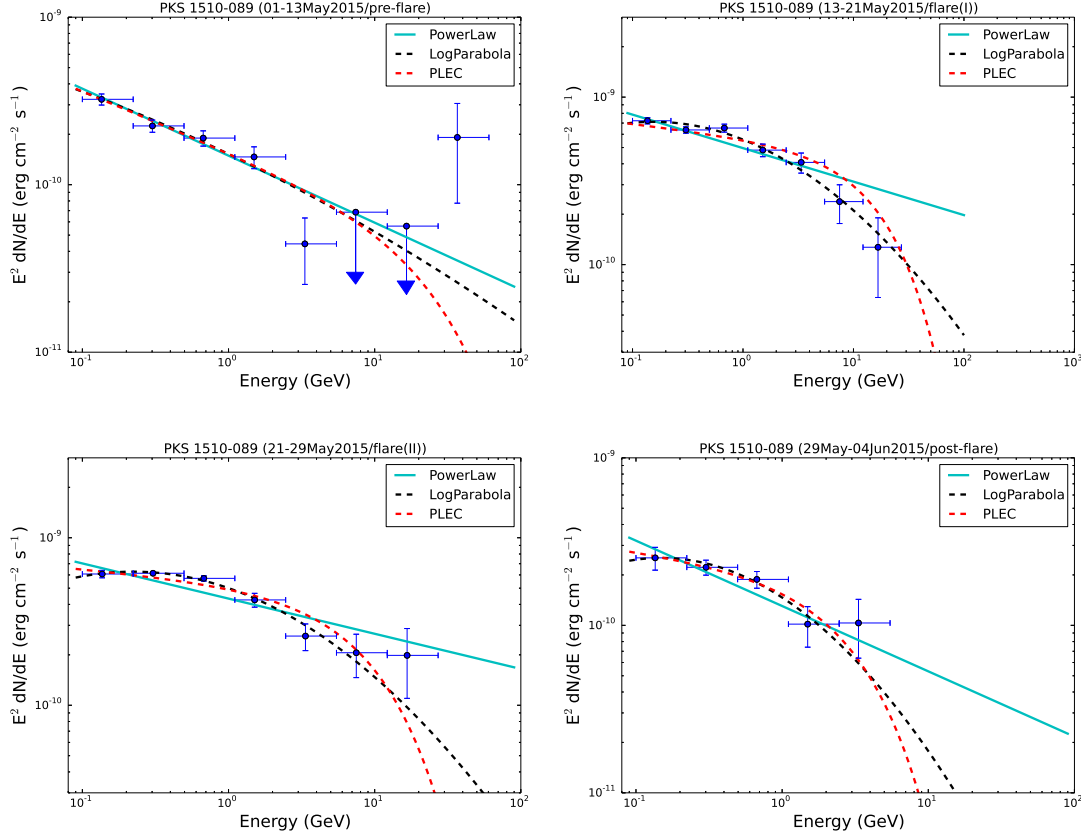


**Figure 24.** Fermi-LAT SEDs during different activity states of flare-4(B) as defined in Fig.11 . PL, LP, PLEC models are shown in cyan, black and red color and there respective parameters are given in the Table-16.

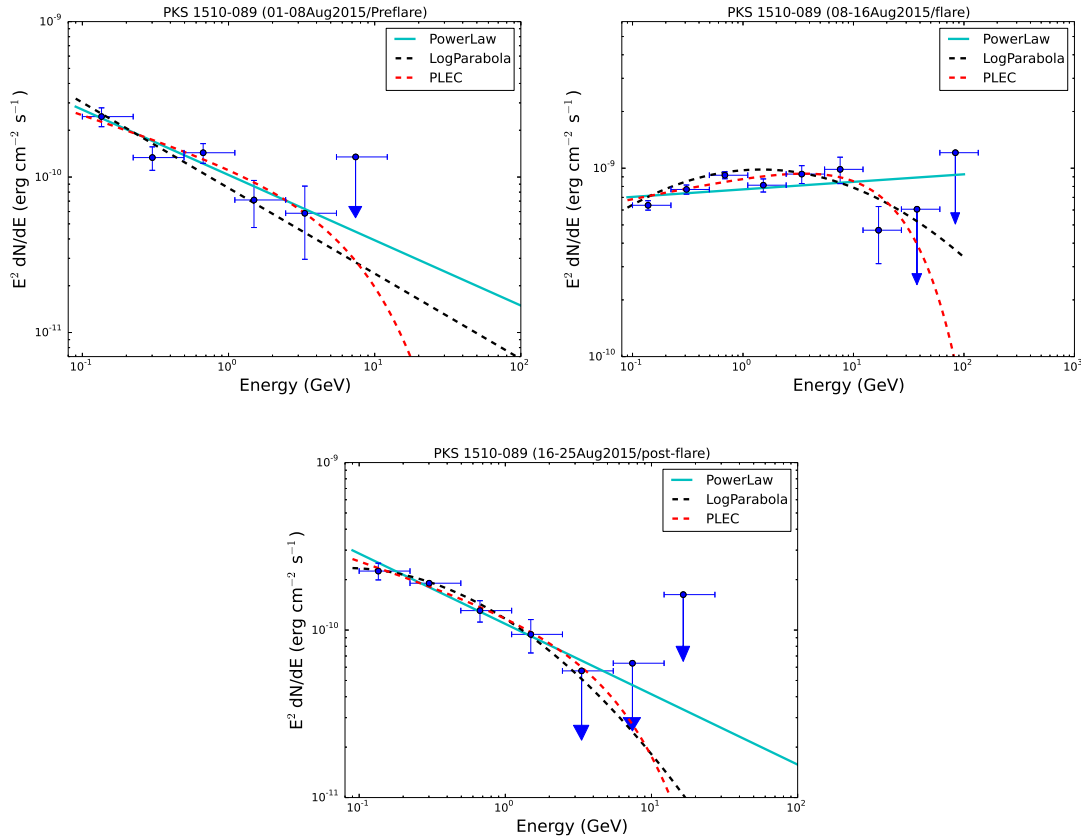


**Figure 25.** Fermi-LAT SEDs during different activity states of flare-4(C) as defined in Fig.12 . PL, LP, PLEC models are shown in cyan, black and red color and there respective parameters are given in the Table-17.

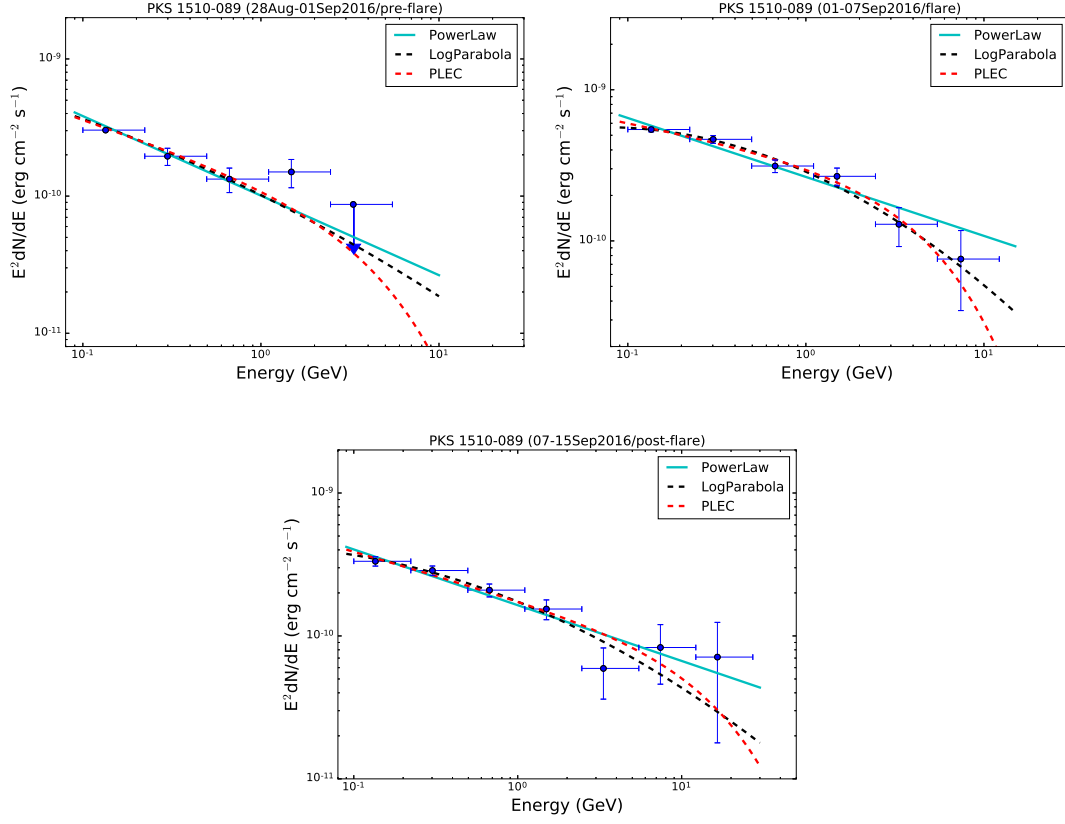


**Figure 26.** Fermi-LAT SEDs during different activity states of Flare-5 as defined in Fig.13 . PL, LP, PLEC models are shown in cyan, black and red color and there respective parameters are given in the Table-18.

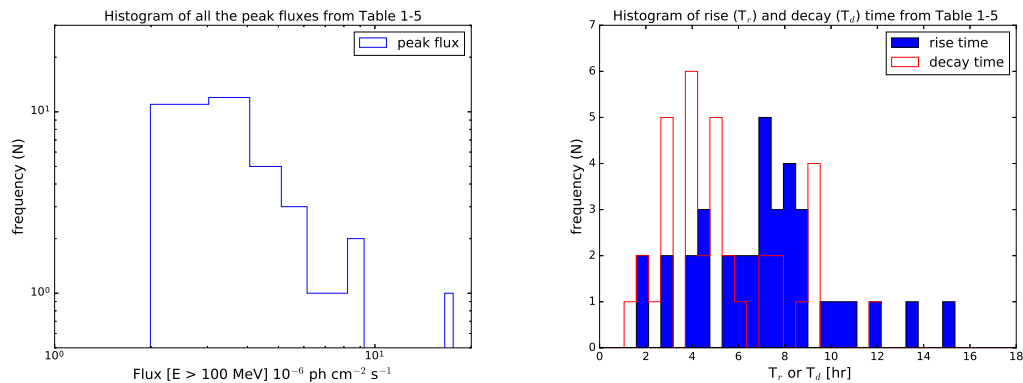


**Figure 27.** Left panel: Histogram of peak fluxes from Tables 1-5. The mean flux is  $3.54 \pm 0.08$  and the standard deviation of the sample is 1.69. Right panel: Histogram of rise and decay time from Tables 1-5. Their mean values are  $6.04 \pm 0.22$  hr and  $3.88 \pm 0.16$  hr respectively. The sample standard deviations are 2.40 hr and 2.20 hr.

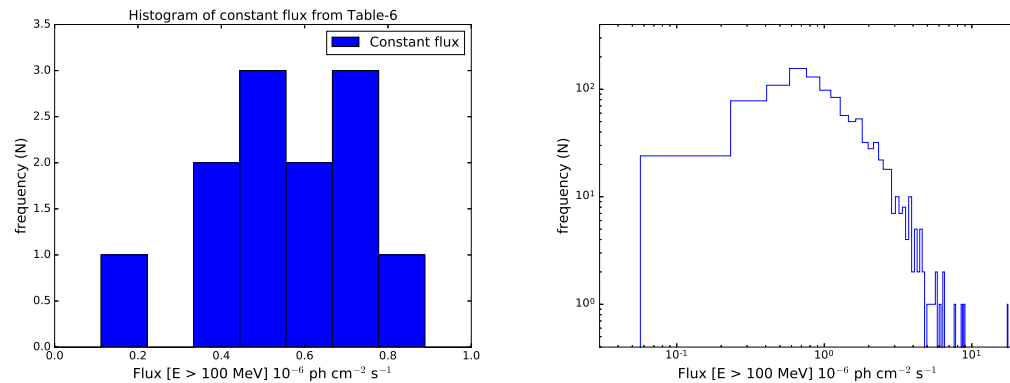


**Figure 28.** Left panel: Histogram of constant flux from Table-6. The mean constant flux is found to be  $0.51 \pm 0.01$  and the standard deviation is 0.20. Right panel: Histogram of all the flux data points. The distribution is peaked, with slow rise up to peak and fast decay after that.

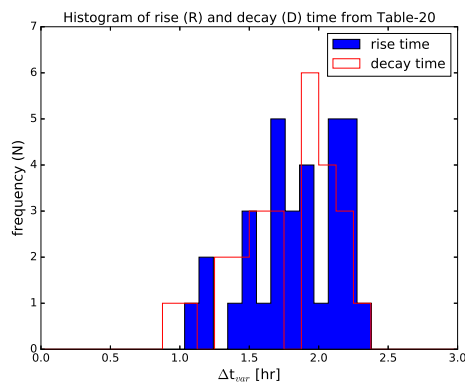


**Figure 29.** Histogram of the rise and decay time from the fastest variability time, Table-20. They are distributed with mean of  $1.75 \pm 0.02$  hr and  $1.76 \pm 0.02$  hr and standard deviation of 0.35 hr, 0.40 hr respectively.